HEAT TRANSFER FLUIDS

DOI: 10.1615/AnnualRevHeatTransfer.2012004122
SOURCE: Lenert, Andrej, Youngsuk Nam, and Evelyn N. Wang. "Heat Transfer Fluids." Annual Review of Heat Transfer 15, 2012.

(Solar Thermal)
Heat Transfer Fluids

Andrej Lenert[1], Youngsuk Nam[1,2], and Evelyn N. Wang[1]

[1]Device Research Laboratory
Department of Mechanical Engineering
Massachusetts Institute of Technology
77 Massachusetts Avenue
Cambridge, MA 02139

[2]Department of Mechanical Engineering
Kyung Hee University
Yongin 446-701, Korea

Abstract

The choice of heat transfer fluids has significant effects on the performance, cost and reliability of solar thermal systems. In this chapter, we evaluate existing heat transfer fluids such as oils and molten salts based on a new figure of merit capturing the combined effects of thermal storage capacity, convective heat transfer characteristics and hydraulic performance of the fluids. Thermal stability, freezing point and safety issues are also discussed. Through a comparative analysis, we examine alternative options for solar thermal heat transfer fluids including water-steam mixtures (direct steam), ionic liquids/melts and suspensions of nanoparticles (nanofluids), focusing on the benefits and technical challenges.

DOI: 10.1615/AnnualRevHeatTransfer.2012004122
SOURCE: Lenert, Andrej, Youngsuk Nam, and Evelyn N. Wang. "Heat Transfer Fluids." Annual Review of Heat Transfer 15, 2012.

DOI: 10.1615/AnnualRevHeatTransfer.2012004122
SOURCE: Lenert, Andrej, Youngsuk Nam, and Evelyn N. Wang. "Heat Transfer Fluids." Annual Review of Heat Transfer 15, 2012.

Nomenclature

a	ratio of heated perimeter to perimeter
A	area (m^2)
C_k	coefficient of k enhancement ($Wm^{-1}K^{-1}$)
C_p	specific heat capacity at constant pressure ($Jkg^{-1}K^{-1}$)
C_μ	coefficient of μ enhancement ($kgm^{-1}s^{-1}$ or Pa s)
d	particle diameter (nm)
D	diameter (m)
E	heat transfer enhancement factor
Fr	Froude number
g	gravitational acceleration (ms^{-2})
G	Total mass flux through a tube ($kgm^{-2}s^{-1}$)
h	heat transfer coefficient ($Wm^{-2}K^{-1}$), height (m), enthalpy (Jkg^{-1})
k	thermal conductivity ($Wm^{-1}K^{-1}$)
K	permeability (m^2)
L	length (m)
m''	mass flux ($kgm^{-2}s^{-1}$)
M	two-phase flow pressure drop multiplier
Mo	Mouromtseff number
Nu	Nusselt number
p	perimeter (m)
P	pressure (Pa)
Pr	Prandtl number
q''	heat flux (Wm^{-2})
r	radius (m)
Re	Reynolds number
S	heat transfer correction factor
T	temperature (K)
u	velocity (ms^{-1})
V	averaged bulk velocity (ms^{-1})

DOI: 10.1615/AnnualRevHeatTransfer.2012004122
SOURCE: Lenert, Andrej, Youngsuk Nam, and Evelyn N. Wang. "Heat Transfer Fluids." Annual Review of Heat Transfer 15, 2012.

We	Weber number
x	vapor quality

Greek symbols

α	thermal diffusivity (m^2s^{-1})
β	tilt angle (^{o})
θ	angle (^{o})
Λ	dimensionless thermal load
μ	dynamic viscosity ($kgm^{-1}s^{-1}$)
ρ	density (kgm^{-3})
Y	dimensionless pumping load
ϕ	volume fraction of solid phase
v	kinematic viscosity (m^2/s)

Subscript

c	capillary
eff	effective
f	fluid
g	gas
h	hydraulic diameter
in	inlet
l	liquid
le	assuming the entire flow as liquid
max	maximum
out	outlet
p	particle
ph	phase
$pool$	pool boiling
s	surface
w	wall

DOI: 10.1615/AnnualRevHeatTransfer.2012004122
SOURCE: Lenert, Andrej, Youngsuk Nam, and Evelyn N. Wang. "Heat Transfer Fluids." Annual Review of Heat Transfer 15, 2012.

DOI: 10.1615/AnnualRevHeatTransfer.2012004122
SOURCE: Lenert, Andrej, Youngsuk Nam, and Evelyn N. Wang. "Heat Transfer Fluids." Annual Review of Heat Transfer 15, 2012.

1. Introduction

Heat transfer fluids serve one or more purposes in solar thermal applications, such as: collection and transport of heat from solar absorbers; intermediate storage of thermal energy to buffer the diurnal nature of solar radiation; and heat exchange with the power cycle to produce electricity. As a result of the multiple purposes of heat transfer fluids in these applications, many constraints, both performance and practical, influence the choice of heat transfer fluid. In typical concentrated solar power (CSP) applications, heat transfer fluids are required to have low freezing points (near room temperature) to avoid freezing overnight, high operating temperatures (>400^{o}C) to increase the power cycle efficiency, and low vapor pressures at high temperatures to reduce installation costs. For heat transfer performance, fluids are expected to have high thermal conductivity, high volumetric heat capacity, and low viscosity. They also need to be environmentally benign, non-corrosive, safe and cost-effective. Since pure substances and commonly used fluids such as synthetic oils and molten salts rarely meet all of the practical and performance criteria, the development of new solar heat transfer fluids continues to be an active area of research. Two of the most commonly pursued research avenues include: mixtures, such as multi-component salts; and composite fluids, such as suspensions of submicron-sized solid particles in liquids (*i.e.*, nanofluids). New developments have been discovered in the recent years in the field of mixtures and composite fluids which can potentially lead to significant breakthroughs for solar thermal applications.

The purpose of this chapter is to review and analyze existing heat transfer fluids and recent advances in the area. A new figure of merit is derived based on the assumption of forced turbulent convection inside a uniformly heated collector tube in *Section 2: Figure of Merit*. More commonly used heat transfer fluids such as water, gases, oils, and molten salts are evaluated based on the new figure of merit in *Section 3: Conventional Heat Transfer Fluids.* *Section 4: Direct Steam* focuses on the performance and practical issues regarding the use of pressurized water-vapor in solar plants. Recent advances in the promising fields of ionic fluids (such as molten salt mixtures) and composite fluids are discussed in *Section 5: Ionic Liquids and Melts* and *Section 6: Nanofluids*, respectively.

DOI: 10.1615/AnnualRevHeatTransfer.2012004122
SOURCE: Lenert, Andrej, Youngsuk Nam, and Evelyn N. Wang. "Heat Transfer Fluids." Annual Review of Heat Transfer 15, 2012.

2. Figure of Merit

2.1 PREVIOUS STUDIES

The choice of proper heat transfer fluids is essential for the development of high-efficiency solar thermal power plants, as it determines the thermal and hydraulic performance of the collector field. Previously, Becker [1] evaluated various heat transfer fluids for use in solar thermal power plants by comparing their individual thermophysical properties. However, the performance of heat transfer fluids is determined by the combination of the properties rather than by each of the individual properties. To evaluate the effects of combined thermophysical properties, researchers have suggested various figures of merit (FOMs). Mouromtseff introduced the Mouromtseff number (*Mo*) to evaluate the effects of combined fluid properties on the convective heat transfer coefficient of internal turbulent flow based on the Dittus-Boelter correlation [2]:

$$Mo = \frac{\rho^{0.8} c_p^{0.33} k^{0.67}}{\mu^{0.47}} \quad . \tag{1}$$

Bonilla suggested another FOM by comparing the required pumping power to maintain the temperature difference between inlet and outlet of carrier fluid [3]:

$$\frac{\rho^2 c_p^{2.8}}{\mu^{0.2}} \quad . \tag{2}$$

Even though these FOMs provide meaningful comparisons among various heat transfer fluids, there are several limitations. Mouromtseff [2] compared only heat transfer characteristics in the radial direction assuming that all fluids have the same flow velocity. Meanwhile, Bonilla [3] ignored radial heat transfer between the wall and the fluid and only considered axial heat flow. Since performance of solar thermal heat transfer fluids is determined by the combined effects of the thermal storage capacity of the fluid, convective heat transfer from the wall to the fluid and hydraulic performance characterized by pumping power, an alternative FOM is desired.

Recently, Murakami and Mikić reported the optimization of heat sinks based on the minimization of pumping power assuming the same temperature difference between wall outlet

DOI: 10.1615/AnnualRevHeatTransfer.2012004122
SOURCE: Lenert, Andrej, Youngsuk Nam, and Evelyn N. Wang. "Heat Transfer Fluids." Annual Review of Heat Transfer 15, 2012.

and fluid inlet [4]. Their approach introduced dimensionless pumping and thermal loads, and showed important relationships among the parameters to optimize heat sink designs considering the axial and radial heat flow as well as the pumping power requirement. Here, we use the methodology suggested by Murakami and Mikić [4] to develop a new FOM to evaluate the performance of conventional solar thermal heat transfer fluids.

2.2 NEW FIGURE OF MERIT

Figure 1 shows a schematic of a solar collector tube which is simplified as a single channel of diameter *D* and length *L*. The heat flux is assumed to be uniform throughout the entire length and the temperature distribution inside the solid walls is neglected.

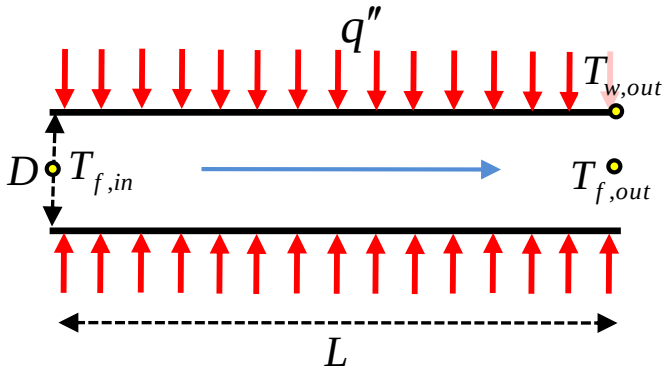

Figure 1: Schematic of a solar collector tube simplified as a single channel of diameter *D* and length *L*; $T_{f,in}$ and $T_{f,out}$ represent the inlet and outlet temperature of carrier fluid, respectively. $T_{w,out}$ is the outlet wall temperature.

From conservation of energy, the amount of heat stored in the fluid can be described as:

$$\rho VAc_p(T_{f,out} - T_{f,in}) = q''apL \quad , \tag{3}$$

where *V* and *p* represent the average bulk velocity of fluid and the perimeter of tube, respectively. *a* is the correction factor for the case when the heat flux is applied to a fraction of the perimeter. For solar thermal collector tubes, the thermal stability of the heat transfer fluid and the selective coating imposes a restriction on $T_{w,out}$. Therefore, we rewrite Eq. 3 using the maximum temperature difference between the tube wall and fluid inlet ($\Delta T_{max} = T_{w,out} - T_{f,in}$):

$$T_{f,out} - T_{f,in} = (T_{w,out} - T_{f,in}) - (T_{w,out} - T_{f,out}) = \Delta T_{\max} - \frac{q''}{h} \quad . \tag{4}$$

Then, the pumping power is normalized by the amount of heat transferred to the fluid per time:

$$\overline{P} = \frac{\Delta PVA}{q''apL} = \frac{1}{8a}\frac{Y}{\Lambda}\frac{f\,\mathrm{Re}^3}{\overline{D}^3} \quad , \tag{5}$$

where $\overline{D}$ is a normalized diameter (D/L), f is the internal friction factor, and Re is the Reynolds number. Y and Λ represent the dimensionless pumping and thermal loads, respectively:

$$\begin{aligned} Y &\equiv \frac{\rho v^3}{k\Delta T_{\max} L^2} \\ \Lambda &\equiv \frac{q''L}{k\Delta T_{\max}} \end{aligned} \quad . \tag{6}$$

Eqs. 3 and 6 are substituted into Eq. 4:

$$1 = \frac{\Lambda\overline{D}}{Nu} + F \quad , \tag{7}$$

where F is a normalized temperature rise of the fluids, $(T_{f,out} - T_{f,in})/\Delta T_{\max}$, described by:

$$F \equiv \frac{4a\Lambda}{\mathrm{Re}\cdot\mathrm{Pr}} \quad . \tag{8}$$

For turbulent flow in circular tubes, the internal friction factor and the *Nusselt* number (Nu) can be estimated as [5, 6]

$$\begin{aligned} f &= 0.184\,\mathrm{Re}^{-0.2} \\ Nu &= 0.023\,\mathrm{Re}^{0.8}\,\mathrm{Pr}^{0.4} \end{aligned} \quad . \tag{9}$$

By substituting Eqs. 6-9 into Eq. 5:

$$\overline{P} \propto \left(\frac{\mathrm{Y}\Lambda^{2.4}}{\mathrm{Pr}^{1.6}}\right)\left(\frac{1}{F^{0.4}(1-F)^3}\right). \tag{10}$$

DOI: 10.1615/AnnualRevHeatTransfer.2012004122
SOURCE: Lenert, Andrej, Youngsuk Nam, and Evelyn N. Wang. "Heat Transfer Fluids." Annual Review of Heat Transfer 15, 2012.

Assuming the heat flux (q''), tube length (L) and the maximum temperature difference between the tube wall and fluid inlet ($\Delta T_{\max}$) are fixed, the normalized pumping power is determined by the properties of the fluid and the Reynolds number. To elucidate the effect of fluid properties on the normalized pumping power without introducing complexity associated with the Reynolds number, we optimize the normalized temperature rise (F):

$$\frac{\partial}{\partial F}\left(\frac{1}{F^{0.4}(1-F)^{3}}\right)=0\,. \tag{11}$$

By substituting the optimized F (= 2/17) into Eq. 10, the normalized pumping power can be described:

$$\overline{P}\propto\left(\frac{\mu^{1.4}}{\rho^{2.0}c_p^{1.6}k^{1.8}}\right)\left(\frac{q''^{2.4}}{\Delta T_{\max}^{3.4}}\right)L^{0.4}\,. \tag{12}$$

Then, the performance of heat transfer fluids is determined by the combination of fluid properties in the first parentheses. Since the normalized pumping power needs to be minimized, the FOM of solar thermal heat transfer fluids becomes:

$$FOM=\frac{\rho^{2.0}c_p^{1.6}k^{1.8}}{\mu^{1.4}}\,. \tag{13}$$

2.3 SUMMARY & OUTLOOK

A new FOM is suggested to evaluate the thermal and hydraulic performance of heat transfer fluids for solar thermal applications. Compared with the *Mo* number (Eq. 1), the suggested FOM (Eq. 13) has a strong dependency on ρ and c_p which characterize the heat storage capacity of fluid. In addition, unlike the previous FOM (Eq. 2), the thermal conductivity of fluid k also has a strong effect as the new FOM includes heat transfer characteristics between wall and fluid in the radial direction. When the carrier fluids experience phase-change in the collector tube, the changes in thermal and hydraulic performance associated with the phase-change process need to be considered.

DOI: 10.1615/AnnualRevHeatTransfer.2012004122
SOURCE: Lenert, Andrej, Youngsuk Nam, and Evelyn N. Wang. "Heat Transfer Fluids." Annual Review of Heat Transfer 15, 2012.

3. Conventional Heat Transfer Fluids

In addition to the FOM discussed in Section 2, the choice of fluid for solar thermal applications is governed by many other practical considerations. The commonly available heat transfer fluids for solar thermal power plants are summarized in Table 1. For large scale solar thermal plants (*e.g.*, Solar Energy Generating Systems), synthetic or mineral oils have been the most common heat transfer fluid due to their high stability over a relatively wide temperature range (15°C – 400°C) [7, 8]. The use of molten salts that are stable at higher temperatures (> 400°C) has also been suggested by previous studies to enhance the power cycle efficiency [9].

Table 1: Conventional and potential heat transfer fluids for solar collector fields.

		Fluid
Oils	Synthetic	Therminol® VP-1[10]
	Mineral	Caloria HT 43 [1]
Molten salts	Nitrates	Hitec® [11], Hitec® Solar Salt [11]
	Chlorides	KCl-$MgCl_2$ [12]
	Fluorides	LiF-NaF-KF (FLiNaK) [12]
Other liquids		Mercury [13]
		Water [14]
Pressurized gases		Water vapor (30 - 100 bar) [14]
		Air (30-100 bar) [15]

Figure 2 shows the thermophysical properties and the FOM of the various heat transfer fluids listed in Table 1. Volumetric heat capacity (Figure 2a), thermal conductivity (Figure 2b), and dynamic viscosity (Figure 2c) values are shown, and the combined effects of these properties (Figure 2d) are evaluated using the FOM discussed in Section 2.

3.1 EVALUATION OF HEAT TRANSFER FLUIDS

Between the two types of oils, the synthetic oil performs better than the mineral oil due to its higher thermal conductivity and lower viscosity. Therminol® VP-1 has been the most common heat transfer fluid used in parabolic trough solar plants; however, its modest thermal breakdown temperature (~400^{o}C) limits the efficiency of power cycles [8].

Between the oils and the salts, the molten salts have a higher FOM due to their higher volumetric heat capacity and thermal conductivity. At 325^{o}C, for example, the FOM of nitrate salts (*e.g.*, Hitec®, Hitec® Solar Salt) is approximately two and nine times higher than the synthetic (*e.g.*, Therminol® VP-1) and mineral oil (*e.g.*, Caloria HT 43), respectively. Fluoride molten salts (*e.g.*, FLiNaK) have higher energy density and thermal conductivity than the nitrate ones, but the higher viscosity limits their overall benefit. At very high temperatures (> 525^{o}C), the FOM of fluoride salts becomes larger than that of the nitrate salts due to the decrease in viscosity. However, the freezing point (> 425^{o}C) is too high for existing solar thermal applications.

Molten salts have a potential to improve both the collector field and power cycle efficiencies due to their higher FOM compared with the oil-based heat transfer fluids. Moreover, molten salts are cheaper and environmentally less harmful than the oils. However, the high freezing point of the molten salts requires a freeze protection method in the solar field, which increases the operation and maintenance cost. For example, Hitec® freezes at ~140ºC [11] while the synthetic oil usually freezes at ~15ºC. To further reduce the freezing point of molten salts, recent studies have introduced advanced molten salt mixtures based on nitrate/nitrite anions [16]. Details of the recent progress in multi-component molten salts and ionic liquids will be discussed in *Section 5: Ionic Liquids and Melts*.

Water and water-vapor are also promising heat transfer fluids for solar thermal plants, as shown in Figure 2d. In fact, alternative solar thermal plants using water and water-vapor as heat transfer fluids have been successfully operated for more than 4000 hours through the Direct Solar Steam (DISS) project [17]. The alternative system, the so-called direct steam generation (DSG) solar thermal plants, will be separately discussed in *Section 4: Direct Steam*.

Gases such as air are also promising heat transfer fluids due to their extremely low viscosity and cost. The volumetric heat capacity can be increased by increasing the operating pressure. However, the increase in working pressure may raise the cost of solar field piping.

DOI: 10.1615/AnnualRevHeatTransfer.2012004122
SOURCE: Lenert, Andrej, Youngsuk Nam, and Evelyn N. Wang. "Heat Transfer Fluids." Annual Review of Heat Transfer 15, 2012.

3.2 OPERATING TEMPERATURE

Figure 2d shows that the performance of heat transfer fluids is strongly temperature-dependent. For the presented liquids, the FOM rapidly increases as the temperature increases mainly due to the rapid decrease in viscosity (Figure 2b). For the gases, the trend is reversed; the FOM decreases with temperature, primarily because the volumetric capacity decreases rapidly as the temperature increases (Figure 2a).

The operating temperature also affects the power cycle efficiency since an increase in fluid outlet temperature increases the Rankine cycle efficiency of steam turbines. For typical concentrated solar power (CSP) plant designs, power cycle efficiency increases from 37.6% to 40% by increasing the solar field fluid outlet temperature from ~390ºC to ~450ºC [9].

Despite the benefits of increasing the operating temperature, the thermal stability of fluids and selective coatings on collector tubes sets an upper limit on the fluid temperature. The Luz System Three (LS-3) collector tube, utilized in the most recent SEGS and DISS plants, is only stable up to ~400°C [18, 19]. Two new selective coatings with interface stacks and cermet layers stable up to ~450°C were recently developed within the DISS project but have not been applied yet [17]. Therefore, the operating temperature of fluids should be carefully determined considering the entire system, including the collector tubes, the power block steam turbine, and the fluid itself.

3.3 SAFETY AND RELIABILITY

Other characteristics of the heat transfer fluids including flammability, toxicity and corrosiveness also need to be considered for the safe and reliable operation of solar plants. For the collector fields using highly flammable heat transfer fluids such as oils, fire extinguishing systems are required to protect the solar plants against fire hazards. In fact, the first SEGS plant using mineral oil was destroyed in 1999 by a fire. In subsequent SEGS plants, mineral oil was replaced by less flammable synthetic oil [20]. Even though mercury has a very high FOM (see Figure 2d), the use of mercury is not suggested because mercury and most of its compounds are extremely toxic. For solar plants using molten salts, the collector tubes need to be corrosion resistant. At elevated temperature (~450°C), molten salts may corrode some metals including steel, stainless

DOI: 10.1615/AnnualRevHeatTransfer.2012004122
SOURCE: Lenert, Andrej, Youngsuk Nam, and Evelyn N. Wang. "Heat Transfer Fluids." Annual Review of Heat Transfer 15, 2012.

steels and copper. The corrosion rates of various metals by nitrate salts (*e.g.*, Hitec®) are provided by manufacturers [11].

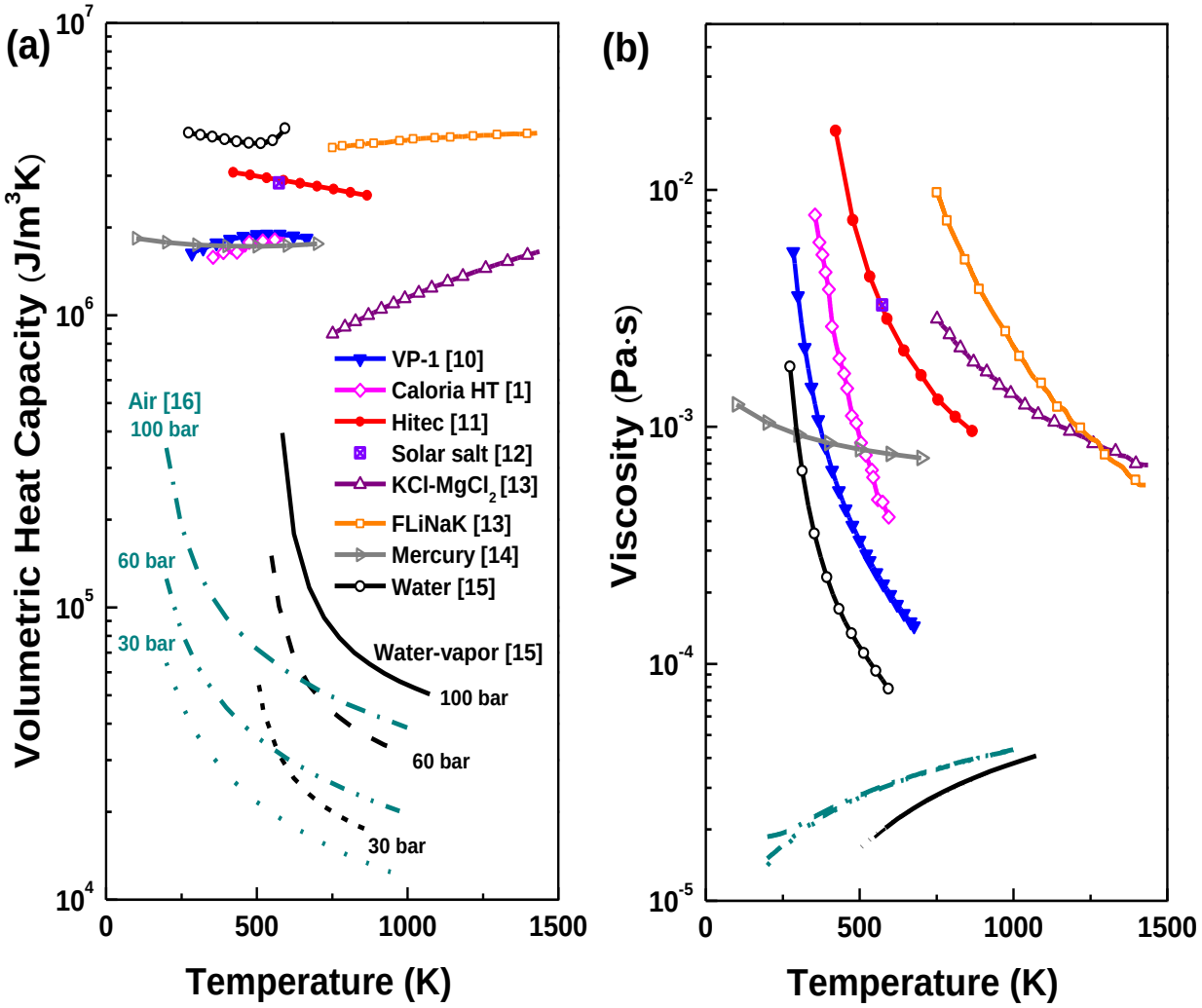

DOI: 10.1615/AnnualRevHeatTransfer.2012004122
SOURCE: Lenert, Andrej, Youngsuk Nam, and Evelyn N. Wang. "Heat Transfer Fluids." Annual Review of Heat Transfer 15, 2012.

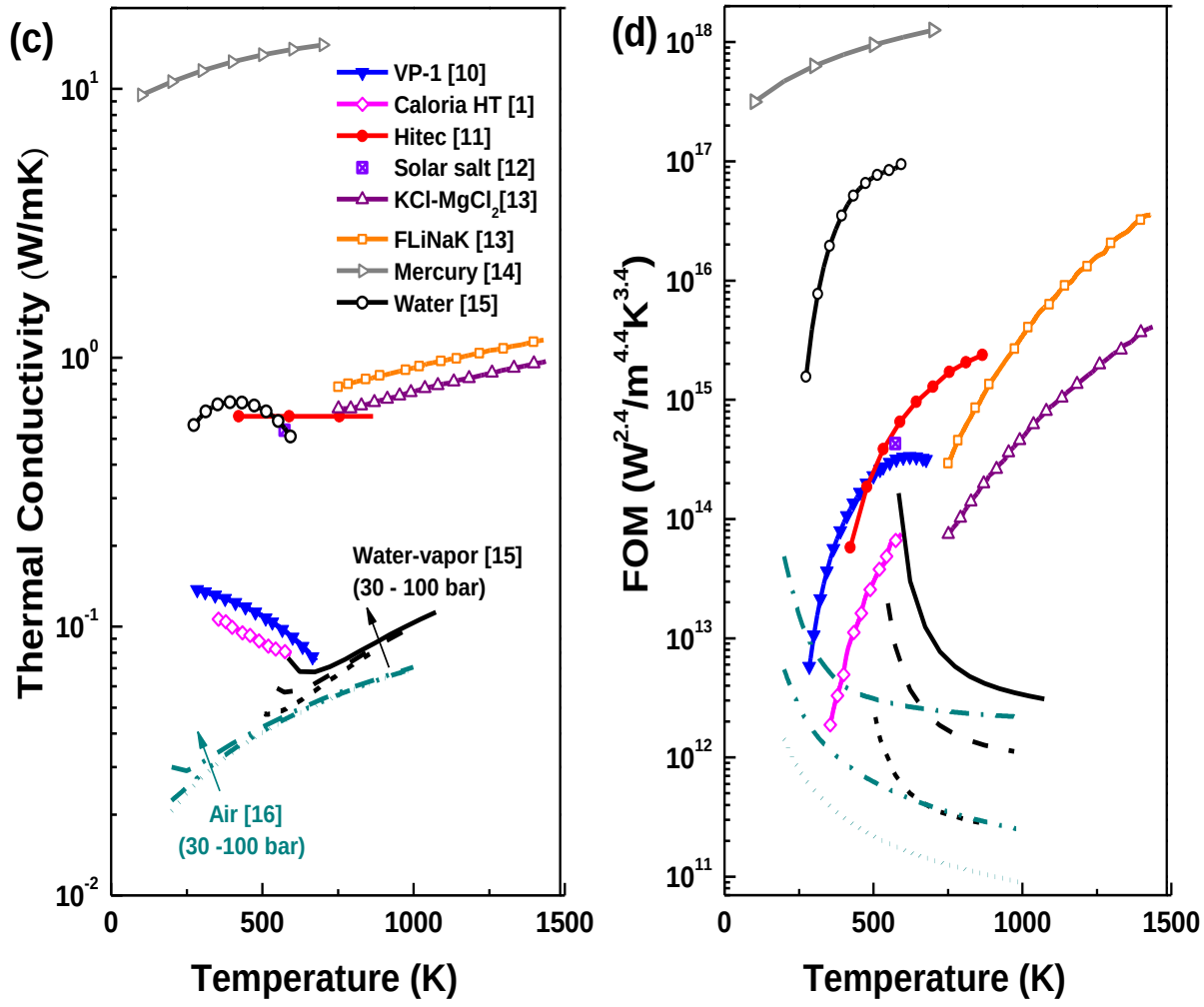

Figure 2: Thermophysical properties and FOM of heat transfer fluids: (a) volumetric heat capacity, (b) dynamic viscosity, (c) thermal conductivity, (d) figure of merit (FOM). $P_l = P_{sat}(T)$ and $P_g = 30 – 100$ bar.

3.4 SUMMARY & OUTLOOK

The performance of various heat transfer fluids is evaluated for solar thermal applications based on the individual thermophysical properties and the new FOM. The comparison shows that molten salts should perform better than oil-based fluids. However, several technical issues including freeze protection and the selection of proper materials for piping need to be considered

DOI: 10.1615/AnnualRevHeatTransfer.2012004122
SOURCE: Lenert, Andrej, Youngsuk Nam, and Evelyn N. Wang. "Heat Transfer Fluids." Annual Review of Heat Transfer 15, 2012.
to successfully apply the molten salts to large scale solar plants. Pressurized gases including air and water vapor are also promising economical heat transfer fluids but the levelized electricity cost (LEC) should be investigated considering the high pressure requirement in the collector tube.

4. Direct Steam

Conventional parabolic trough solar thermal power plants are built with two separate thermal cycles for collecting solar radiation and converting it to electricity. The solar collector field utilizes a heat transfer fluid that flows through collector tubes and the power block converts the absorbed solar thermal energy to electricity using a water-steam cycle. The two cycles are connected *via* a heat exchanger which transfers energy from the intermediate heat transfer fluid to the water-steam circuit. Solar thermal power plants using oil-based heat transfer fluids have been successfully demonstrated through the well-known SEGS projects [7]. However, the oil-based heat transfer fluids are thermally unstable over ~400°C [8], flammable, environmental unfriendly and relatively expensive; thus limiting the system efficiency and the dollar per watt metric.

To overcome these limitations, direct steam generation (DSG) solar thermal plants using a water-steam mixture as the heat transfer fluid have been suggested. In the DSG plants, feed-water is preheated and evaporated inside the collector tubes, which provides an additional increase in volumetric heat capacity due to the latent heat of vaporization. At the collector outlets, superheated or saturated steam directly enters the power block water-steam turbine without experiencing an additional heat exchanging process (Figure 3). The outlet steam temperature can be higher than that of oil-based heat transfer fluids. Therefore, DSG solar plants may potentially improve both solar collector field performance and power cycle efficiency. Even with the high pressure requirement in the collector tube, the overall investment cost may decrease since DSG systems do not require heat exchangers and additional elements associated with the intermediate heat transfer fluid including the costly fluid itself. The environmental risk and fire hazard in case of leaks also decrease.

Despite the promise, the implementation of the DSG technology requires a full understanding of technical issues and potential problems associated with the hydrodynamic behavior of two-phase flow and the high pressure requirements in the collector field. In order to overcome the lack of knowledge and to investigate the technical and commercial feasibility of the DSG, a complete R&D program (DISS project) was initiated in 1995 [17, 21, 22]. The DISS test facility was

implemented at the *Plataforma Solar de Almeria* (PSA) in 1997 and successfully operated for more than 4000 hours. Through the DISS project, the feasibility of DSG systems has been proven under real solar conditions and reliable models have been developed based on the collected data. The experiences acquired during the DISS project were applied in the development of the first pre-commercial DSG solar power plant within the Integration of DSG Technology for Electricity Production (INDITEP) project [23] which provided detailed engineering for DSG systems focusing on high operation flexibility and reliability.

Unlike the conventional heat transfer fluids discussed in Section 3, water used in DSG solar fields experiences a transient phase-change process inside the collector tube. As a result, the performance of solar fields strongly depends on the changes in flow regime inside the tubes and cannot be evaluated using the FOM (Eq. 13) for single-phase fluids. In this section, we discuss the important parameters determining the thermal and hydraulic performance of the DSG collector fields based on empirical two-phase flow correlations and experimental data obtained from the DISS project.

4.1 STEAM GENERATION MODE

Schematics of DSG solar fields operating under three different steam generation modes are shown in Figure 3a.

In the once-through mode, all of the water introduced at the collector is preheated, evaporated, and converted into superheated steam during the circulation through the collector rows. Due to its simplicity, this process minimizes the investment cost; however, control of the outlet steam temperature is challenging [24].

In the injection mode, small fractions of feed water are injected along the collector row. This process provides good control of the superheated steam at the outlet. The complexity of the system, however, may increase the investment cost.

In the recirculation mode, feed water is injected at a higher flow rate compared with the other modes and only a fraction of the water is converted into steam. A water-steam separator placed at the end of the evaporating section separates steam from the water and then the remaining water is transferred back to the collector inlet by a recirculation pump.

DOI: 10.1615/AnnualRevHeatTransfer.2012004122
SOURCE: Lenert, Andrej, Youngsuk Nam, and Evelyn N. Wang. "Heat Transfer Fluids." Annual Review of Heat Transfer 15, 2012.

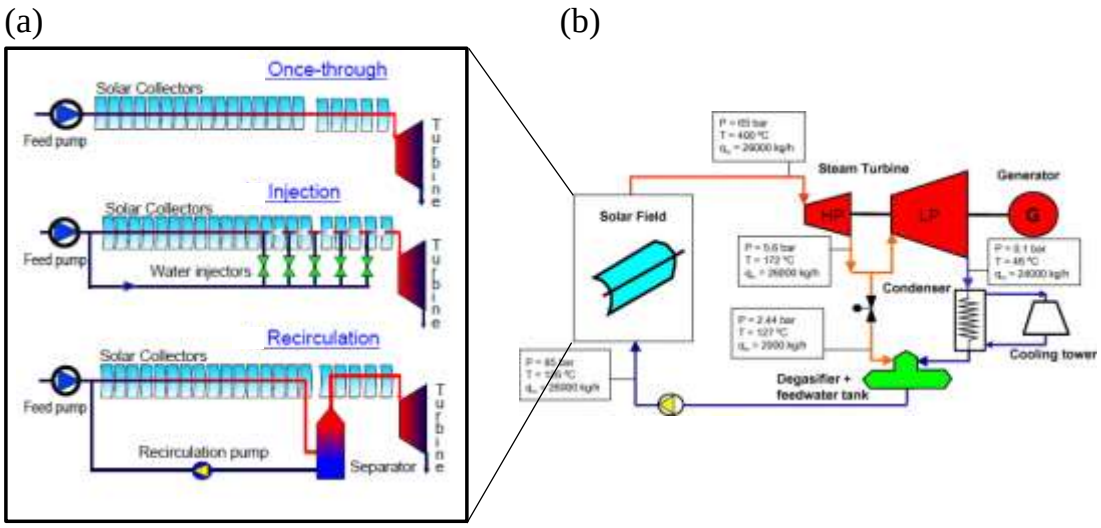

Figure 3: Schematics of DSG solar thermal power plants: (a) solar field showing three configurations and (b) power block (for the 5MWe INDITEP DSG). Adapted from [22] (Copyright 2002, ASME) and [23] (Copyright 2006, Elsevier), respectively.

One of the main tasks of the DISS project was to determine the best steam generation mode among the three options. Within the project, the controllability of the once-through and the recirculation modes was compared under real transient solar conditions. The test of the injection mode could not be completed due to a failure of the devices required for running the injection mode [17]. Measured temporal changes in outlet temperature of the DISS test loop are shown in Figure 4 with measured direct normal irradiation (DNI) [24]. Under similar solar inputs, the recirculation mode better regulated the outlet steam temperature compared with the once-through mode due to the presence of the water-steam separator damping the disturbances. Details on the control schemes applied for each mode are described in [25]. More sophisticated adaptive controllers will improve the controllability of the once-through process but they will increase the investment and management cost. Even though the test could not be completed, it has been discussed that the injection mode also requires a more sophisticated controller than the simple proportional-integral-derivative (PID) algorithm applied to the DISS plant [26]. Based on the experience obtained from the DISS project, the recirculation mode was determined the best among the three configurations. Table 2 shows the specifications of the DISS solar field using the recirculation mode.

DOI: 10.1615/AnnualRevHeatTransfer.2012004122
SOURCE: Lenert, Andrej, Youngsuk Nam, and Evelyn N. Wang. "Heat Transfer Fluids." Annual Review of Heat Transfer 15, 2012.

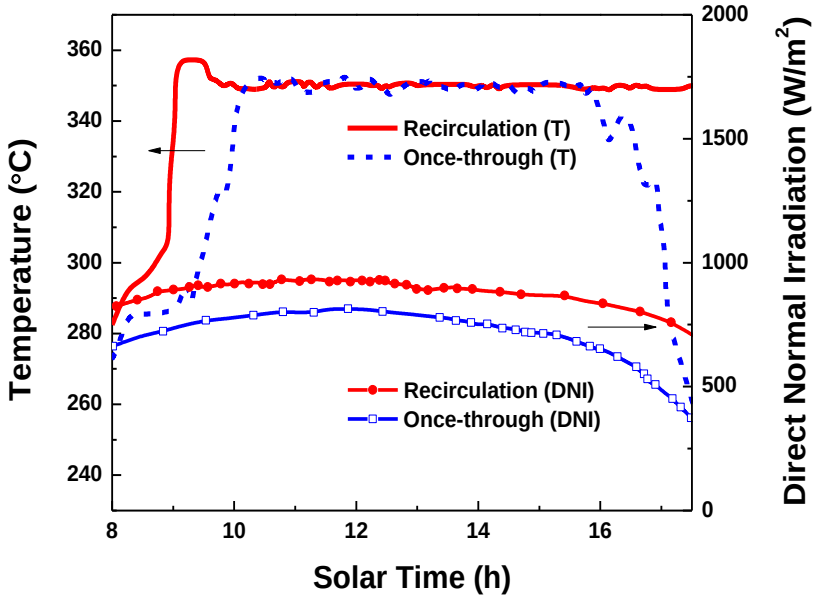

Figure 4: Temporal changes in the collector outlet temperature and the direct normal irradiation (DNI) of the DISS collector loop with recirculation (in red / July 5th, 2001) and once-through (in blue / July 11th, 2001) steam generation modes. Adapted from [24] (Copyright 2003, Elsevier).

Table 2: Specifications of the DISS solar field [17].

Number of parabolic trough modules	40
Total row length	550 m
Collector tube inner/outer diameter	50 / 70 mm
Steam mass flow per row	0.8 kg / s
Maximum water recirculation rate ($m''_{recirculation} / m''_{steam}$)	4
Maximum outlet steam temperature/pressure	400 ºC / 100 bar

4.2 FLOW PATTERNS

The two-phase flow patterns inside the collector tubes play a significant role in the determination of the heat and mass transfer performance. To increase the efficiency and the reliability of collector fields, it is critical to prevent the formation of a stratified flow zone. The presence of flow stratification results in a non-uniform heat transfer coefficient distribution along the perimeter and introduces large circumferential temperature gradients, which may lead to

DOI: 10.1615/AnnualRevHeatTransfer.2012004122
SOURCE: Lenert, Andrej, Youngsuk Nam, and Evelyn N. Wang. "Heat Transfer Fluids." Annual Review of Heat Transfer 15, 2012.
collector tube damage. In the annular flow region, a thin-film of water that covers the entire wall provides a high heat transfer coefficient and low temperature gradient around the entire wall.

Previous studies [27-29] have suggested a model for predicting flow transitions in horizontal two-phase flow, considering stratified flow with a wave existing on the surface. As the gas accelerates, the pressure in the gas phase decreases and the wave grows. Then, the transition from stratified to annular or intermittent flow can be determined by the Kelvin-Helmholtz instability. For a round pipe, the criterion is represented by the following dimensionless form [29]:

$$Fr^2\left[\frac{1}{(1-\tilde{h}_l)^2}\frac{\tilde{u}_g d\tilde{A}_l / d\tilde{h}_l}{\tilde{A}_g}\right] \geq 1 \qquad Fr = \sqrt{\frac{\rho_g}{(\rho_l - \rho_g)}}\frac{u_g^s}{\sqrt{Dg\cos\beta}} \quad , \qquad (14)$$

where Fr is the Froude number modified by the density ratio. The definition of A_g, A_l, h_l, u_g, β are graphically shown in Figure 5 (length and area were normalized with D and D^2, repectively). The superficial gas velocity u_g^s is normalized with u_g.

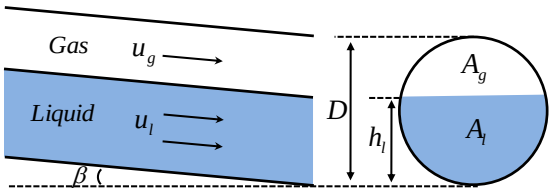

Figure 5: The schematic of equilibrium stratified flow; a liquid flows along the bottom of a tube and a gas flows separately above the liquid. A and u represent the cross-sectional area and flow velocity of each phase, respectively. β is a tilt angle of the tube. Reproduced from [29].

When the flow satisfies the criterion (Eq. 14), two possible flow regimes can occur. If the supply of liquid is large enough, a stable slug can form (*i.e.*, intermittent flow); otherwise, the wave is swept up around the wall and annular flow takes place, *i.e.*, the liquid level in the stratified flow

determines whether intermittent or annular flow will occur. It has been suggested that when the liquid level in the tube is below the center line ($h_l / D \leq 0.5$), annular flow occurs [27, 29].

During the DISS project, it was observed that the flow inside the DSG collector tube is mainly wavy or annular. Based on the experimental data, an empirical correlation has been developed that predicts the mass flux value where the transition from wavy to annular flow occurs for various heat fluxes in DSG applications [30]:

$$m_g'' = (46.6 + 0.595P + 0.119P^2)\left(1 + 1.3\frac{q''}{56}\right) \quad , \qquad (15)$$

where P and q'' are given in bar and kW/m^2, respectively, and the mass flux is calculated in kg/(m^{2}s).

To increase the portion of annular flow, a small degree of inclination of the absorber tubes has been suggested [28, 29]. Downward inclinations can decrease the stratified and intermittent flow region by increasing the liquid velocity and decreasing the liquid level. The influence of the tilt on the temperature gradients inside the absorber tubes was experimentally investigated under real solar conditions within the DISS project. The ninth collector tube was tilted by 4° and the maximum circumferential temperature difference was measured at four different locations with varying operating pressure (30 bar – 100 bar) and steam quality (0.4 – 1) [17, 22]. The results showed that the benefit of the inclination was not significant since the horizontal tubes already satisfied the reliability criteria. In two-phase flow regions, the maximum temperature difference along the perimeter was measured to be <30 K in both horizontal and tilted tubes. Considering the increase in cost associated with tilting, the study recommended using horizontal tubes without inclination [24].

4.3 HEAT TRANSFER COEFFICIENT

Based on the prediction of the flow patterns, the overall heat transfer performance can be estimated with semi-empirical correlations developed for different flow regimes. Researchers have developed convective heat transfer correlations for saturated flow boiling inside horizontal

DOI: 10.1615/AnnualRevHeatTransfer.2012004122
SOURCE: Lenert, Andrej, Youngsuk Nam, and Evelyn N. Wang. "Heat Transfer Fluids." Annual Review of Heat Transfer 15, 2012.
tubes with relatively high Reynolds numbers. The details of the correlations are summarized in Table 3.

When feed-water enters or superheated vapor exits the tube, the water or vapor is heated only by single-phase convective heat transfer. In this preheating or superheated zone, the heat transfer coefficient can be predicted from the Dittus-Boelter correlation [6]. Once phase change occurs, the flow pattern can be determined using the criteria described earlier (Eq. 14 or 15). In the stratified flow zone, the increase in the heat transfer coefficient is mainly due to the enhancement in the convective heat transfer since flow must accelerate due to the decrease in fluid density during vaporization. Shah described the heat transfer coefficient of stratified flow by multiplying the single-phase flow convective heat transfer coefficient (h_{1ph}) by an enhancement factor (E_{Shah}) [31] :

$$h_{2ph} = E_{Shah} h_{1ph} = 3.9 Fr_{le}^{0.24} \left(\frac{x}{1-x} \right)^{0.64} \left(\frac{\rho_l}{\rho_g} \right)^{0.4} h_{1ph} \quad , \qquad (16)$$

where h_{1ph} can be calculated from the Dittus-Boelter correlation with the modified Reynolds number: $\mathrm{Re}_l = \frac{G(1-x)D_h}{\eta}$.

When the transition to the annular or intermittent flow occurs, boiling on the tube inner wall provides additional heat transfer enhancement. In these regimes, the overall heat transfer coefficient can be described as the sum of convective and boiling contributions [32-34]:

$$h_{2ph} = E_{Chen} h_{1ph} + S h_{pool} \quad , \qquad (17)$$

where h_{pool} can be determined from the Forster and Zuber correlation for nucleate pool boiling [35]. E_{Chen} (> 1) is an enhancement factor for the convective contribution (similar with E_{Shah} in Eq. 16) and S (< 1) is a correction factor reflecting the lower effective superheat available in forced convection compared with pool boiling [36].

DOI: 10.1615/AnnualRevHeatTransfer.2012004122
SOURCE: Lenert, Andrej, Youngsuk Nam, and Evelyn N. Wang. "Heat Transfer Fluids." Annual Review of Heat Transfer 15, 2012.

Using a similar concept, Kandlikar proposed a general correlation applicable to a wide range of fluids and flow conditions [37]. It has been reported as one of the most reliable general correlations:

$$h_{2ph} = h_{1ph}\left[C_1 Co^{C_2}(25Fr_{le})^{C_5} + C_3 Bo^{C_4} F_K\right] . \quad (18)$$

Since the measured heat transfer coefficients inside the DSG collector tubes are not available, the evaluation of different correlations for DSG applications has not yet been reported. Most of previous studies have applied Chen's correlation (Eq. 17) to model the heat transfer characteristics of two-phase flow inside the DSG collector tubes [30, 38].

In order to provide additional enhancement of heat transfer in the collector tube, the integration of capillary systems such as porous coatings or micro channels has been proposed [39]. The capillary systems pull the water to the top of the tube via capillary forces, which prevents flow stratification and increases the overall heat transfer coefficient. For capillary structures of small effective pore diameters, inertial effects are small and the volumetric flow rate per cross-sectional area (u) is described as:

$$u(\theta_l) = \frac{K}{\mu_l R\theta_l}\left(\frac{2\sigma\cos\theta_s}{r_c} - \rho_l gR(1-\cos\theta_l)\right) \quad , \quad (19)$$

where K and r_c represent the permeability and the capillary radius of the porous media, respectively. θ_s is the contact angle, R is the inner radius and θ_l is the wetting front position (Figure 6). When the capillary force generated by the porous media becomes smaller than the viscous and gravitational forces, dryout occurs inside the capillary structures. The maximum external heat flux that keeps the internal surface of the pipe wet up to the angular position θ_l without dryout is:

$$q_{\max}(\theta_l) = \frac{t_{coating}\rho_l h_{fg}}{4\alpha_{tube}} u(\theta_l)^2 \quad , \quad (20)$$

DOI: 10.1615/AnnualRevHeatTransfer.2012004122
SOURCE: Lenert, Andrej, Youngsuk Nam, and Evelyn N. Wang. "Heat Transfer Fluids." Annual Review of Heat Transfer 15, 2012.

where $t_{coating}$ and α_{tube} are the thickness of the porous media and the thermal diffusivity of the tube, respectively.

DOI: 10.1615/AnnualRevHeatTransfer.2012004122
SOURCE: Lenert, Andrej, Youngsuk Nam, and Evelyn N. Wang. "Heat Transfer Fluids." Annual Review of Heat Transfer 15, 2012.

Table 3: Flow boiling correlations applicable to the DSG collector fields.

<table>
<tr><th></th><th colspan="2">Heat transfer coefficient</th><th>Pressure drop</th></tr>
<tr><td>Pre-heating or superheated</td><td colspan="2">$h_{1ph} = 0.023\mathrm{Re}^{0.8}\,\mathrm{Pr}^{0.4}\frac{k}{D_h}$ [6]</td><td>$\left(\frac{dP}{dz}\right)_{1ph} = f\frac{l}{d}\frac{\rho v^2}{2}$</td></tr>
<tr><td>Stratified flow</td><td>$h_{2ph} = E_{Shah}h_{1ph}$ [31]
$= 3.9Fr_{le}^{\,0.24}\left(\frac{x}{1-x}\right)^{0.64}\left(\frac{\rho_l}{\rho_g}\right)^{0.4} h_{1ph}$
where $Fr_{le} = \frac{G^2}{\rho_l^2 gD}$ [32, 39]</td><td>$h_{2ph} = h_{1ph}\left[C_1 Co^{C_2}(25Fr_{le})^{C_5} + C_3 Bo^{C_4} F_K\right]$ [37]
where
$Co = \left(\frac{1-x}{x}\right)^{0.8}\left(\frac{\rho_v}{\rho_l}\right)^{0.5}$
$Bo = \frac{q''}{Gh_{lv}}$
$Fr_{le} = \frac{G^2}{\rho_l^2 gD}$
$F_K = 1$ ($for\ water$)
Coefficients :
Co < 0.65 (convective); Co ≥ 0.65 (nucleate boiling)
C_1: 1.1360 / 0.6683
C_2: -0.9 / -0.2
C_3: 667.2 / 1058.0
C_4: 0.7 / 0.7
C_5*: 0.3 / 0.3
* $C_5 = 0$ for vertical tubes and horizontal tubes with $Fr_{le} > 0.04$.</td><td>$\left(\frac{dP}{dz}\right)_{2ph} = M\left(\frac{dP}{dz}\right)_{1ph,l}$ [40]
where
$M = A + 3.43x^{0.685}(1-x)^{0.24}\left(\frac{\nu_g}{\nu_l}\right)^{0.8}\left(\frac{\mu_g}{\mu_l}\right)^{0.22}\left(1-\frac{\mu_g}{\mu_l}\right)^{0.89} Fr_l^{-0.47} We_l^{-0.0334}$
$A = (1-x)^2 + x^2\left(\frac{\nu_g f_g}{\nu_l f_l}\right)^{0.8}$
$Fr_l = \frac{(m\nu_l)^2}{gd_i}$
$We_l = \frac{m^2 d_i \nu_l}{\sigma}$
$f_{g,l} = \frac{64}{\mathrm{Re}_{l,g}}$ $(\mathrm{Re}_{l,g} \le 1055)$
$f_{g,l} = \left[0.86859\log\left(\frac{\mathrm{Re}_{l,g}}{1.964\log(\mathrm{Re}_{l,g}) - 3.8215}\right)\right]^{-2}$ $(\mathrm{Re}_{l,g} > 1055)$</td></tr>
<tr><td>Annular or Intermittent flow</td><td>$h_{2ph} = E_{Chen}h_{1ph} + Sh_{pool}$ [32-34]
where
$h_{pool} = 0.00122\left[\frac{k_l^{0.79} c_{pl}^{0.45}\rho_l^{0.49}}{\sigma^{0.5}\mu_l^{0.29}h_{lv}^{0.24}\rho_v^{0.24}}\right]\cdot$
$[T_w - T_{sat}(P_l)]^{0.24}[P_{sat}(T_w) - P_l]^{0.75}$ [35]
Correction factors:
$E_{Chen}(X_{tt}) = 1$ $for\ X_{tt}^{-1} \le 0.1$
$E_{Chen}(X_{tt}) = 2.35\left(0.213 + \frac{1}{X_{tt}}\right)^{0.736}$ $for\ X_{tt}^{-1} > 0.1$
$S = \left(1 + 2.56\times10^{-6}\,\mathrm{Re}_{2ph}^{1.17}\right)^{-1}$, $\mathrm{Re}_{2ph} = \mathrm{Re}_l\left[E_{Chen}(X_{tt})\right]^{1.25}$
$X_{tt} = \left(\frac{\rho_v}{\rho_l}\right)^{0.5}\left(\frac{\mu_l}{\mu_v}\right)^{0.125}\left(\frac{1-x}{x}\right)^{0.875}$</td><td></td><td></td></tr>
</table>

DOI: 10.1615/AnnualRevHeatTransfer.2012004122
SOURCE: Lenert, Andrej, Youngsuk Nam, and Evelyn N. Wang. "Heat Transfer Fluids." Annual Review of Heat Transfer 15, 2012.

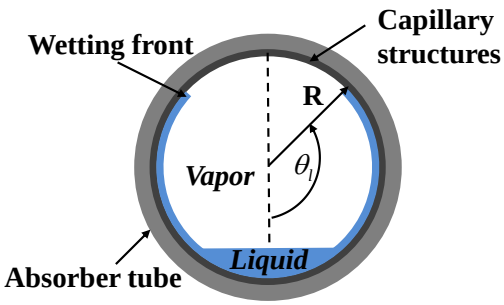

Figure 6: Schematic of a DSG collector tube with internal capillary structures that draw the liquid up to the angular position θ_l.

Once the material for the porous coating and the tube is determined, the capillary structures can be designed considering the operating heat flux range. In general, the increase in the capillary performance factor ($K\cos\theta_s / r_c$) and the thickness of the coating ($t_{coating}$) enhances the maximum heat flux ($q_{\max}$). However, the increase in the coating thickness also increases the thermal resistance. Therefore, structures need to be optimized based on the operating heat flux range to maximize the overall internal heat transfer coefficient.

Suggested internal capillary structures may increase the number of operating hours as they can prevent the formation of flow stratification even at low solar radiation. The increase in the thin evaporative film area can also increase the overall heat transfer coefficient in the absorber tubes. However, the incorporation of capillary structures in DSG absorber tubes has not yet been demonstrated mainly due to the challenges in the fabrication process and the increase in the investment cost.

4.4 PRESSURE DROP

The pressure drop inside the DSG collector loop is also an important performance factor since it determines the pumping power requirement. Methods for predicting the pressure drop in two-phase flow have been classified as homogeneous and separated flow models. The homogeneous flow model assumes two-phase flow as a homogeneous pseudo-fluid characterized by averaged properties of the two phases. Despite its simplicity, this model has been recommended only for

high mass flux (> 2000 kg/m^{2}s) flows [41]. The separate models consider the two-phase flow as separated streams and predict the pressure gradient using a two-phase multiplier. Lockhard and Martinelli [42] originally suggested the prediction method based on a two-phase multiplier, and Martinelli and Nelson [32] extended the study to higher pressure ranges up to the critical pressure. Chawla [43] determined the pressure drop of annular flow considering the friction between the phases and between the fluid and the wall. Friedel's correlation [40] uses a two-phase liquid multiplier assuming the liquid phase flows alone in the channel with the total mass flow rate.

For a DSG collector loop which operates under high pressure and low mass flux conditions (Table 2), the homogeneous model is not suitable. Among the separate models, Martinelli and Nelson [32] or Friedel's correlation [40] have been suggested by previous studies [21, 28, 44]. Friedel's correlation was determined to be best for DSG applications from the data obtained during the DISS project [21, 28, 44].

In the preheating and superheated steam zone, where turbulent single-phase convection occurs, the pressure drop can be calculated using the Darcy–Weisbach equation (Table 3) and various friction factor correlations [45]. For the two-phase flow region, Friedel correlated the friction pressure drop as the product of the single phase water flow and a two-phase flow multiplier M [40]:

$$\left(\frac{dP}{dz}\right)_{2ph} = M\left(\frac{dP}{dz}\right)_{1ph,l}, \qquad (21)$$

where the single-phase pressure drop $(dP/dz)_{1ph,l}$ can be calculated from the Darcy–Weisbach equation assuming the total mass flux is liquid. Detailed information on the two-phase multiplier M is provided in Table 3. Compared with the experimental data obtained under real operating conditions, Friedel's correlation overestimated the pressure drop by approximately 25% [21]. Results from the DISS project suggested that the overestimation can be used as a safety margin for collector designs.

DOI: 10.1615/AnnualRevHeatTransfer.2012004122
SOURCE: Lenert, Andrej, Youngsuk Nam, and Evelyn N. Wang. "Heat Transfer Fluids." Annual Review of Heat Transfer 15, 2012.

Figure 7 shows the pressure drop variation with flow rate in DSG and oil-based collector tubes [28]. The flow rate in DSG collector tubes determines the two-phase flow patterns and the contribution of each phase to the total pressure drop. At low flow rates, the total pressure drop rapidly decreases due to the generation of dry steam. A critical region may exist between P_{c1} and P_{c2} where the total pressure drop decreases with increasing flow rate (Ledinegg instability). Another previous study also noticed the possible existence of the critical region in DSG collector tubes and suggested the use of a positive displacement pump to avoid the Ledinegg instability [46]. Therefore, the instability issue should be considered when deciding the flow rate. The pressure drop in the DSG collector tubes (flow rate of ~1 kg/s and D_i = 54 mm) is approximately half of that in the typical oil-based ones (flow rate of 5.5~6.5 kg/s and D_i = 66 mm [28]), which significantly reduces the pumping power requirement.

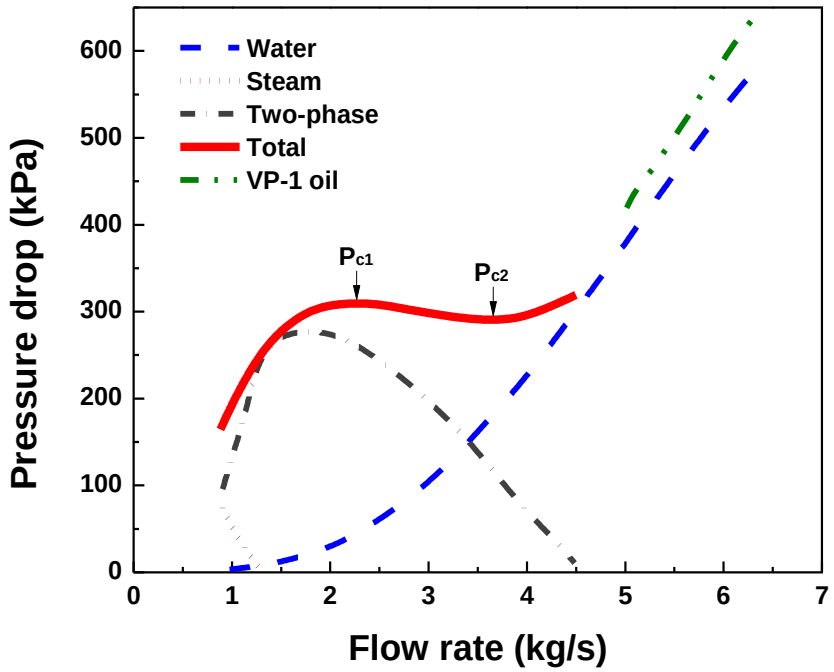

Figure 7: Pressure drop in horizontal DSG and oil-based collector tubes, L_{tube} = 600 m, $D_{i,DSG}$ = 54 mm, $D_{i,oil}$ = 66 mm, T_{in} = 210°C, P_{DSG} = 100 bar, q_{solar} = 1000 W/m^2. Adapted from [28] (Copyright 2000, ASME).

DOI: 10.1615/AnnualRevHeatTransfer.2012004122
SOURCE: Lenert, Andrej, Youngsuk Nam, and Evelyn N. Wang. "Heat Transfer Fluids." Annual Review of Heat Transfer 15, 2012.

4.5 SUMMARY & OUTLOOK

The use of a water-steam mixture as a heat transfer fluid in solar collector fields is a promising method to increase the efficiency and reduce cost. Based on the results of the DISS project, the levelized electricity cost (LEC) of DSG plants operating at 400 ºC and 120 bars was estimated to be 7.7-11.1% lower than that of SEGS-like plants using synthetic oils [47]. By increasing the operating temperature from 400 ºC to 500 ºC, the total LEC reduction can reach up to 10.9-14.1% [47]. For the successful commercialization of the DSG solar plants, the following issues need to be further explored: the optimization of collector loop and power cycle design, the development of new absorber coatings for high temperature, the regulation of the outlet temperature and pressure, and the reduction of collector piping costs.

5. Ionic Liquids and Melts

Compared to synthetic oils which are commonly used in parabolic trough applications, molten salts operate at higher temperatures, have lower vapor pressures, are more environmentally-friendly and less expensive. Recent feasibility studies have shown that molten salts, serving as both a heat transfer fluid and a storage medium, have the potential to improve performance and lower the overall costs of parabolic trough solar plants [9]. It is envisioned that excess molten salt supplied by the collector loop during periods of high-irradiation can be stored in an insulated tank and later used for power production during periods of low-irradiation (*e.g.*, extended periods of cloud cover, nighttime, *etc*.). Moreover, the ability to increase the operating temperature ($> 450^{o}$C) of the system translates into more efficient thermal-to-electrical conversion in the power cycle [9, 16, 48].

The feasibility of molten salts as heat transfer fluids and storage media has been successfully demonstrated in CSP applications with central receiver designs. Nevertheless, the primary issue preventing the widespread use of molten salt is their relatively high freezing point. During periods of limited or no solar irradiation, the ambient temperature can drop well below 25^{o}C resulting in solidification of the molten salts which ultimately leads to damage of the piping and increased costs associated with thawing [16]. Freeze prevention mechanisms, including overnight circulation of the fluid, auxiliary heaters and heat trace wire, are needed in such systems [9].

To eliminate the solidification problems, current research efforts aim to lower the freezing point of ionic fluids. For this purpose, ionic liquids and multi-component salts have received a significant amount of interest. The difference between ionic liquids and ionic melts (*i.e.*, molten salts) is subtle: ionic liquids, by definition, have freezing point temperatures below the boiling point of water. Furthermore, ionic liquids typically have organic cations, while molten salts are composed of inorganic anions and cations [49]. The focus of this section is to review and discuss recent advances in both ionic liquids and multi-component salts for use in solar thermal applications, most of which have targeted lowering the freezing point and extending the working range of the fluid.

DOI: 10.1615/AnnualRevHeatTransfer.2012004122
SOURCE: Lenert, Andrej, Youngsuk Nam, and Evelyn N. Wang. "Heat Transfer Fluids." Annual Review of Heat Transfer 15, 2012.

5.1 MULTI-COMPONENT SALTS

The melting point of binary and ternary mixtures is significantly lower as compared to the pure components because of increased entropy when mixed. In a simple binary mixture system, a particular composition of the two components (*i.e.*, eutectic point) will minimize the freezing point (or liquidus temperature). For this reason, salts currently used in solar thermal applications such as Hitec® and Hitec® Solar Salt are eutectic binary or ternary mixtures. Liquidus temperatures as low as 108°C for eutectic mixtures of nitrate/nitrite anions with two alkaline cations have been reported [50].

Recent work has focused on extending this concept by investigating multi-component salt mixtures. In such systems, the phase diagram can be significantly more complex and harder to predict [51]; hence, a combinatorial experimental approach has been adopted to determine the composition with the lowest melting point.

As shown in the phase diagram in Figure 8, Cordaro *et al.* investigated a mixture of cations of sodium, potassium and lithium with a fixed 1:1 molar ratio of nitrate/nitrite anions [16]. They were not able to find a eutectic or near-eutectic point, yet they obtained liquidus temperatures below 80°C. By sampling aliquots of the liquid phase during freezing and experimentally determining their composition, a liquidus temperature near 70–75°C for a Li:K:Na (30%:50%:20%) salt with a nitrate/nitrite ratio of approximately 0.56 was obtained.

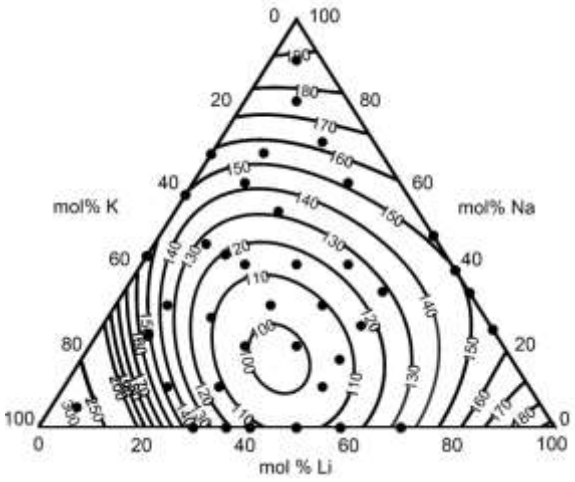

Figure 8: Phase diagram for Li:Na:K mixture with nitrate/nitrite (1:1 molar ratio). (Dots: experimental data; Lines: mathematically interpolated.) From [16] (Copyright 2011, ASME).

Bradshaw *et al.* [51] investigated nitrate/nitrite systems with sodium, potassium, lithium and calcium cations. Calcium nitrate was found to lower the liquidus temperature moderately and significantly increase the viscosity of the melt. Lithium nitrate, on the other hand, was found to reduce the liquidus temperature significantly and have a weak effect on viscosity.

The thermal stability of nitrate/nitrite multi-component salts is expected to be limited by the oxidation of nitrite into nitrate. As nitrate is formed, the mixture shifts away from the eutectic point elevating the freezing point such that insoluble products may form in the heat transfer fluid which clog the valves and pipes [51]. An inert atmosphere can prevent this problem since the nitrite/nitrate reaction is governed by the partial pressure of oxygen in contact with the molten salts. The thermal stability of nitrate/nitrite multi-component salts in air is expected to be similar to existing nitrate/nitrite salts (*i.e.*, ~500^{o}C). Thermal decomposition of these salts at high temperatures yielding different types of oxides is also a concern since soluble oxide ions can increase the amount of corrosion [51].

A limited amount of research currently exists on the thermophysical properties and heat transfer performance of low melting point multi-component salt mixtures. Moreover, the cost of lithium containing salts is high; low-cost substitutes for lithium need to be investigated if the fluid is to be used as a thermal storage medium.

5.2 IONIC LIQUIDS

In contrast to molten salt mixtures where the freezing point is decreased via the addition of salts with small and polarizing inorganic cations (*e.g.*, Li), ionic liquids have large and asymmetrical organic cations [52]. Although other cations have been synthesized and used in ionic liquids, the imidazolium cation ([im]) and its derivatives have been prevalent in research because of their low melting points which are attributed to the asymmetrical nature of [im] [52]. Moreover, properties of ionic liquids (such as the melting point) can be tuned through modification of the chemical group attached to the basic [im] structure [48]; examples of which are shown in Figure 9.

DOI: 10.1615/AnnualRevHeatTransfer.2012004122
SOURCE: Lenert, Andrej, Youngsuk Nam, and Evelyn N. Wang. "Heat Transfer Fluids." Annual Review of Heat Transfer 15, 2012.

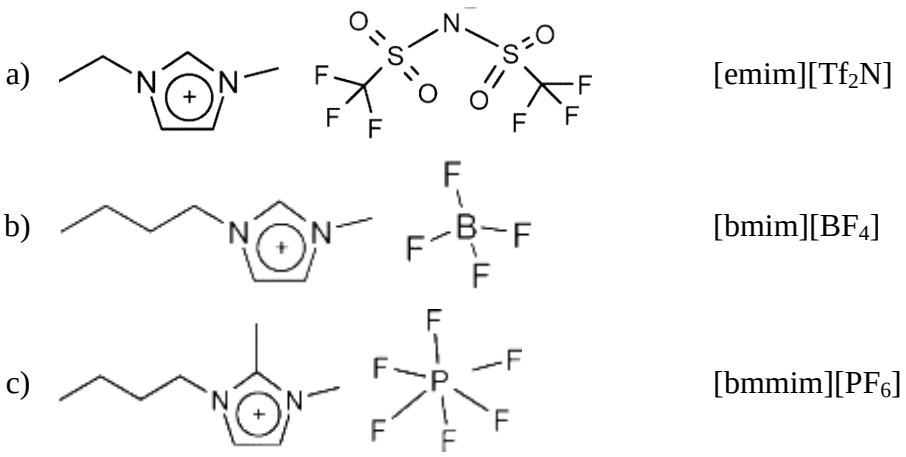

Figure 9: Chemical structure of the following imidazolium-based ionic liquids: a) 1-*n*-ethyl-3-methylimidazolium bis(trifluoromethylsulfonyl)imide, [emim][Tf_2N]; b) 1-*n*-butyl-3-methylimidazolium tetrafluoroborate, [bmim][BF_4]; c) 1-*n*-butyl-2,3-dimethylimidazolium hexafluorophosphate, [bmmim][PF_6]. Adapted from [53] (Copyright 2004, American Chemical Society).

Van Valkenburg studied several "common" [im]-based ionic liquids for use as HTFs in solar thermal applications [49]: 1-methyl-3-ethylimidazolium tetrafluoroborate ([emim][BF_4]), 1-methyl-3-butylimidazolium tetrafluoroborate ([bmim][BF_4]), and 1,2-dimethyl-3-propylimidazolium bis(trifluorosulfonyl)imide ([dmpi]Im). The thermophysical properties of these ionic liquids are summarized in Table 4. The thermal conductivity, heat capacity and density of the three ionic liquids are comparable and similar to the properties of synthetic oils such as Therminol® VP-1; the viscosity of the ionic liquids, however, is at least an order of magnitude higher.

When evaluated on the basis of the FOM discussed in Sections 1 and 2, the heat transfer performance of the three [im]-based ionic liquids in Table 4 is relatively poor (~10^{11}-10^{12}) and comparable to low-pressure air or water-vapor. The increased viscosity severely limits the applicability of these ionic liquids, especially in parabolic trough applications where the pressure drop is a concern because of the relatively long solar collector loop.

DOI: 10.1615/AnnualRevHeatTransfer.2012004122
SOURCE: Lenert, Andrej, Youngsuk Nam, and Evelyn N. Wang. "Heat Transfer Fluids." Annual Review of Heat Transfer 15, 2012.

Table 4: Summary of thermophysical properties and temperature ranges for three ionic liquids [49].

Property	***Ionic Liquids***		
	[emim][BF_4]	[bmim][BF_4]	[dmpi]Im
Density, 60º C (kgm^{-3})	1253	1175	1421
Heat capacity, 100º C ($Jkg^{-1}K^{-1}$)	1281	1659	1196
Thermal conductivity, 25°C ($Wm^{-1}K^{-1}$)	0.200	0.186	0.131
Dynamic viscosity, 25°C ($kgm^{-1}s^{-1}$)	0.036	0.120	0.090
$FOM = \frac{\rho^{2.0} c_p^{1.6} k^{1.8}}{\mu^{1.4}}$	8.5 (10^{11})	1.8 (10^{11})	1.3 (10^{11})
Freezing point (°C)	14.4	-87.4	11.3
Thermal decomposition onset (°C)	446	424	457

The ~50°C higher onset of thermal decomposition for [emim][BF_4] compared to Therminol® VP-1 has the potential to increase efficiency in the power cycle and outweigh the cost of the increased pressure drop. Further studies on the feasibility of these and other ionic liquids are needed to confidently assess their applicability in CSP.

The temperature dependence of the thermophysical properties of ionic liquids has been reported by Van Valkenburg and others [49, 53-55]. In general, the heat capacity shows a weak dependence, while the thermal conductivity and density decrease slightly with increasing temperature. Chen *et al.* [55] determined that the viscosity of an imidazolium-based ionic fluid decreases with increasing temperature following an Arrhenius-like behavior; furthermore, their experiments show that the ionic fluid is Newtonian.

Few heat transfer experiments using ionic liquids as the heat transfer fluid exist in literature. Chen *et al.* [55] studied the convective heat transfer behavior of an [im]-based ionic fluid under laminar flow conditions. The thermal entrance length for the ionic fluid was determined to be very large compared to that of water because of the relatively low thermal conductivity and high viscosity of the ionic fluid. The convective heat transfer coefficient over the developing region

correlated well with analytical predictions for their geometry (Shah's equation) but it was significantly lower than that for water under the same conditions. Thus, as predicted by the individually measured properties, the heat transfer performance of many ionic liquids is limited.

5.3 SUMMARY & OUTLOOK

The difference between ionic fluids and ionic melts is becoming less distinct as current research using inorganic multi-component mixtures of salts is successfully lowering the liquidus temperature below 100^{o}C. Research in both areas of ionic liquids and ionic melts will most likely converge toward multi-component systems optimized for heat transfer performance and a wide region of thermal stability. Cost-effective ionic liquids with comparable viscosities to synthetic oils and temperature stability approaching 500^{o}C need to be developed. Similarly, multi-component salts are promising for solar parabolic trough applications but lower cost alternatives to lithium nitrate need to be incorporated.

DOI: 10.1615/AnnualRevHeatTransfer.2012004122
SOURCE: Lenert, Andrej, Youngsuk Nam, and Evelyn N. Wang. "Heat Transfer Fluids." Annual Review of Heat Transfer 15, 2012.

6. **Nanofluids**

In order to enhance the thermophysical properties of common heat transfer fluids, researchers have investigated colloids where solid particles are suspended in a liquid. The basic idea originates from the assumption that the characteristic benefits of two or more components can be combined to achieve the desired properties. In the case of solid-liquid composites for example, the addition of solid particles was proposed to increase the effective thermal conductivity and storage density. However, it was found that solid-liquid composites with larger particles lead to problems with sedimentation, clogging, and erosion in heat transfer applications. Suspensions of submicron-sized solid particles, on the other hand, promise to alleviate some of the aforementioned issues and have recently received a significant amount of attention in literature.

In this section we focus on suspensions of nanoparticles (*i.e.,* nanofluids) including solid nanoparticles and phase-change nanoparticles. Nanofluids have generated much interest in the heat transfer community where order of magnitude thermal conductivity enhancements were experimentally obtained. We discuss the recent advances reported in literature regarding nanofluids and indentify technological issues that need to be overcome before they can be successfully adopted in solar thermal applications. The proposed mechanisms explaining the thermophysical properties of nanofluids are also discussed.

Nanofluids are primarily evaluated based on their performance under turbulent forced convection since those are the conditions most commonly encountered in existing solar collectors. Heat transfer enhancements deviating from predictions based on empirical correlations are discussed.

We will also explore the dual-use potential of nanofluids in solar thermal applications, where in addition to being heat transfer fluids, they can act as volumetric solar receivers, replacing selective surface coatings by directly absorbing solar radiation, or direct storage media, eliminating the need for an intermediate thermal storage medium. These dual-use applications have the potential of increasing the efficiency and reducing the cost of existing systems by eliminating the need for a specific component or loop.

DOI: 10.1615/AnnualRevHeatTransfer.2012004122
SOURCE: Lenert, Andrej, Youngsuk Nam, and Evelyn N. Wang. "Heat Transfer Fluids." Annual Review of Heat Transfer 15, 2012.

6.1 THERMOPHYSICAL PROPERTIES

In this subsection we review the thermal conductivity, viscosity, heat capacity and radiative properties of nanofluids. The properties of solid-liquid composites are conventionally understood using effective medium theories or mixing rule formulations; however, nanofluids have shown behavior not captured by these classical approaches, generating much interest in the research community. Our discussion will focus on currently well-accepted mechanisms explaining the behavior of nanofluids since research in this area remains active and sometimes controversial.

6.1.1 Thermal Conductivity

Effective medium theory is a relatively simple approach used to describe transport properties (*e.g.*, thermal conductivity) of composites. In the limit that the thermal conductivity of the solid particles (k_p) is much higher than that of the basefluid (k_f), the effective conductivity k_{eff} of dilute nanofluids can approximately be described by

$$\frac{k_{eff}}{k_f} \approx 1 + C_k \phi \,, \tag{22}$$

where C_k is the thermal conductivity enhancement coefficient and ϕ is the volume fraction of the solid particles. For a dilute suspension ($\phi < 0.03$) of non-interacting spherical particles, Maxwell obtained that $C_k = 3$ [56]. Additional effects have been incorporated to generalize the effective medium theory such as particle shape and the interfacial resistance between the solid and the basefluid. Descriptions of these effects can be found in past reviews of nanofluids [57-60]. Many investigators have reported experimental data not explained by effective medium theory (EMT) and proposed physical mechanisms beyond EMT to explain the discrepancies and "anomalous" effects [61]. The dominant mechanisms have not been identified primarily due to a lack of agreement between the experimental results of different investigators, however, the main mechanisms discussed in literature are as follows [57]:

i) **Interfacial layering**: Ordering of basefluid molecules at the particle interface and formation of a high-conductivity solid-like interfacial layer (Figure 10a). An *in situ* study of an alumina-aluminum interface using a high-resolution transmission electron microscope provides experimental evidence of ordering of the liquid molecules at a

crystal interface (*i.e.,* interfacial layer), even at elevated temperatures (~750 ^{o}C) [62]. Kaplan and Kauffmann [63] reviewed both theoretical and experimental studies of liquid molecule ordering adjacent to crystalline solids. Gerardi *et al.* [64] observed layering of water (forming a ~1.4 nm thick layer) on alumina particles using NMR, but they did not measure an anomalous conductivity enhancement.

ii) **Agglomeration**: Formation of particle clusters within the basefluid leading to increased effective solid fraction and preferential heat flow through the highly conductive clusters (Figure 10b). Timofeeva *et al.* [65] found that the thermal conductivity was not significantly affected by aggregation, whereas, Wamkam *et al*. [65, 66] observed a significant enhancement of thermal conductivities (>20%) in 3 wt % suspensions when aggregation was most pronounced. Both groups suggest that the reason for the discrepancy lies in the nature and amount of the agglomeration: strong aggregates, which could lead to k_{eff} enhancement; and aggregate-like ensembles, which occur due to weak repulsive forces between particles and are unlikely to enhance k_{eff} because of the solid-liquid-solid interfacial resistance. The effect of agglomeration will be discussed further in the next subsection as it plays an important role in the effective viscosity of nanofluids; more work needs to be done to quantify the effect of agglomeration on thermal conductivity.

DOI: 10.1615/AnnualRevHeatTransfer.2012004122
SOURCE: Lenert, Andrej, Youngsuk Nam, and Evelyn N. Wang. "Heat Transfer Fluids." Annual Review of Heat Transfer 15, 2012.

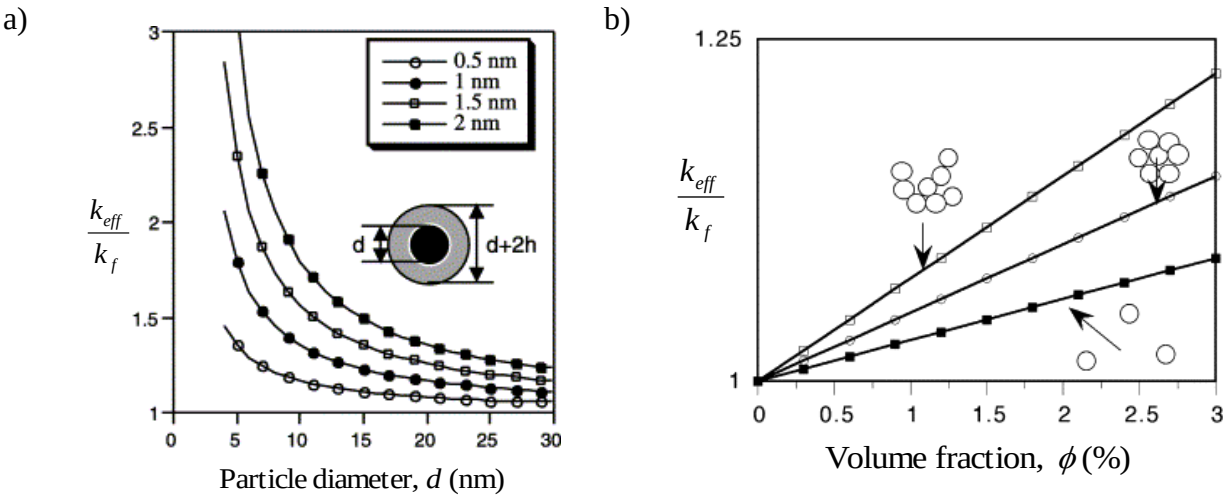

Figure 10: Schematics of mechanisms proposed to explain thermal conductivity enhancement in nanofluids: a) Formation of a highly ordered interfacial layer (h) composed of basefluid molecules around a nanoparticle (diameter, d). Adapted from [67] (Copyright 2002, Elsevier); b) Formation of highly conductive aggregates leading to an increased effective solid volume fraction compared to ϕ of particles (solid squares: well-dispersed particles, circles: packed clusters (60 vol.% particles), open squares: loosely packed clusters (40 vol.% particles). Adapted from [57] (Copyright 2005, Elsevier).

A recent international collaboration (International Nanofluid Property Benchmark Exercise, or INPBE) was coordinated in order to build a consensus in the area. The INPBE had over 30 organizations worldwide measure the thermal conductivity of identical nanofluid samples using several different experimental approaches [68]. Experimental data collected for the INPBE is in good agreement (< 20% error) with the generalized form of the EMT [69] which includes the effects of particle shape and interfacial resistance. A drawback of the generalized EMT formulation, however, is that it has little predictive power since the magnitude of the interfacial resistance (which is not readily available) must be known. Although, the INPBE study observed no anomalous thermal conductivity enhancements and found that proposed theoretical mechanisms such as interfacial layering and agglomeration were not needed to explain the data [68], there is still a debate as to which mechanisms are negligible and which ones can be exploited for thermal conductivity enhancements.

DOI: 10.1615/AnnualRevHeatTransfer.2012004122
SOURCE: Lenert, Andrej, Youngsuk Nam, and Evelyn N. Wang. "Heat Transfer Fluids." Annual Review of Heat Transfer 15, 2012.

At present, the generalized form of the EMT [69] is recommended. Using this formulation, the thermal conductivity enhancement in nanofluids simply increases with increasing particle volume fraction, thermal conductivity (k_p) and aspect ratio. Further systematic studies with explicit control and characterization of the interfacial effects need to be performed to validate any mechanisms beyond the generalized EMT.

6.1.2 Viscosity

Similar to thermal conductivity (Eq. 22), the effective viscosity (μ_{eff}) of nanofluids depends strongly on the volume fraction of nanoparticles in suspension and can be approximately represented by [70]

$$\frac{\mu_{eff}}{\mu_f} \approx 1 + C_\mu \phi \ . \qquad (23)$$

Einstein predicted that for a suspension of non-interacting, hard, uncharged, spherical particles, the coefficient of viscosity enhancement (C_μ) is 2.5 [71]. For non-spherical particles, limitations to rotational and translational Brownian motions lead to higher viscosity. In this case, the coefficient of viscosity enhancement scales with the aspect ratio [70]. In dilute suspensions ($\phi < 0.03$), these formulation were found to work well for particles sizes between 3 and 300 μm, but for suspensions of particles below 500 nm, the experimental viscosity exceeds predictions [72].

An INPBE study on viscosity determined that the measured viscosity dependence on the particle volume fraction for both spherical and non-spherical particles is roughly ten-times larger than predicted (C_μ was 23.4 for spherical particles, and 70.8 for rod-shaped particles) [70]. A slightly lower dependence on ϕ was observed in other studies ($C_\mu \approx$ 4-16). Therefore, models used for micron-size particle suspensions underestimate the viscosity of nanofluids.

The drastically increased viscosity in nanofluids most likely occurs because basefluid molecules are trapped around particles and inside particle clusters leading to an increased effective volume fraction of the solid phase [66, 70, 73]. Electrical double layers and particle-particle interactions govern the formation of effective excluded volumes, as discussed below.

An electrical double layer forms around particles because they typically acquire a surface charge when placed in a liquid. Investigators suggest that the increase in viscosity is proportional to the double layer thickness because molecules in the double layer increase the effective volume of a particle [65, 72-74]. This effective excluded volume effect can play a significant role in small nanoparticles because of their large surface-to-volume ratio.

Agglomeration in nanoparticle suspensions is governed by particle-particle interactions. These interactions are understood as a balance between attractive Van der Waals forces and repulsive electrostatic forces between particles of the same charge. As shown in Figure 11, the balance of these forces can lead to the formation of an energy barrier which reduces contact and aggregation of particles. The influence of surface charge, pH, surfactant additives, particle morphology, and basefluid properties on the particle-particle interactions is discussed in more detail below.

i) **pH:** Adjusting the pH of the nanofluid such that it is further from its isoelectric point (IEP) increases the surface charge of particles and ultimately the repulsive forces, as understood through DLVO theory [66, 75]. Timofeeva *et al.* showed that the viscosity of alumina and SiC nanofluids can be decreased by 31% [65] and by 34% [72], respectively, by controlling the pH of the suspension; while, Wamkam *et al.* [66] lowered the viscosity enhancement ratio from 66% to 20% by changing the pH in ZrO_2 suspensions from 8 to 10 (IEP at pH ≈ 6.2). Both results are explained by the fact that increasing the repulsive forces results in less aggregated suspensions with lower viscosity.

DOI: 10.1615/AnnualRevHeatTransfer.2012004122
SOURCE: Lenert, Andrej, Youngsuk Nam, and Evelyn N. Wang. "Heat Transfer Fluids." Annual Review of Heat Transfer 15, 2012.

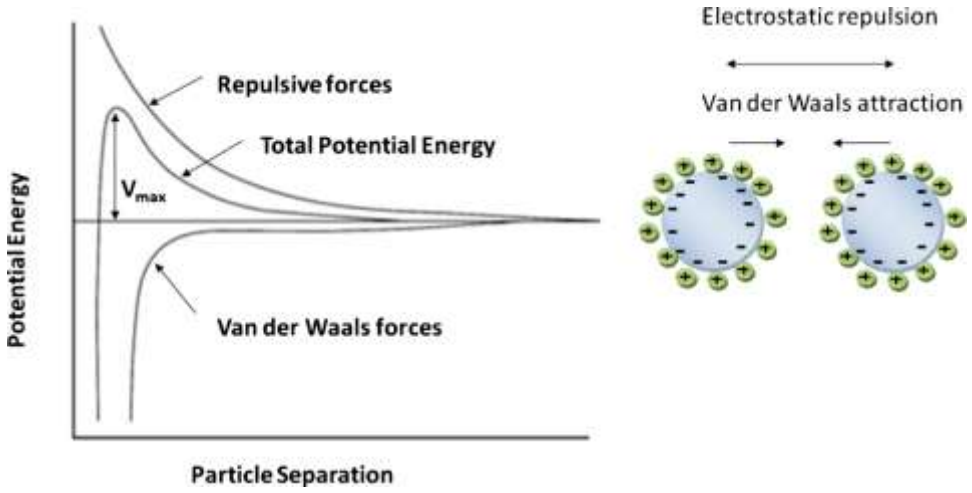

Figure 11: Schematic diagram of the variation in free energy with increasing particle separation, showing a balance between repulsive and attractive forces. From [66] (Copyright 2011, American Institute of Physics).

ii) **Surfactant additives:** Surfactants are typically ligands that adsorb to sites on the nanoparticle surface and impact the repulsive forces between the particles. Surfactants may provide both electrostatic and steric stabilization [74] and improve the viscosity of the suspension. Nevertheless, surfactants are not widely used in solar thermal heat transfer applications because large amounts of surfactant are needed to cover the total nanoparticle interfacial area and the thermal stability of surfactants at elevated temperatures (>200 ^{o}C) has not yet been demonstrated.

iii) **Particle morphology:** the magnitude of the energy barrier preventing nanoparticles from aggregating can be enhanced by increasing the particle size (attractive forces scale with the particle diameter while repulsive forces scale with the diameter squared) [75].

Despite past efforts, the viscosity of nanofluids has yet to be fully connected to DLVO theory and explained using quantitative and predictive models. If agglomeration is accepted as the dominant mechanism, then the viscosity of nanofluids should decrease with increasing repulsion forces between particles and increasing particle size. As discussed, repulsive forces between particles can be tuned using the pH of the suspension. However, practical limitations on pH control and particle size exist such as corrosion and sedimentation, respectively.

6.1.3 Volumetric Heat Capacity

In general, the heat capacity and density of solid-liquid nanofluids is well-predicted using a simple property mixing rule and no dependence on the particle morphology has been observed [72]. The specific heat of nanofluids typically increases or decreases with increasing particle loading depending on whether the nanoparticles have a higher or lower capacity relative to the basefluid [76, 77]. However, a recent study by Shin *et al.* [78] reported an anomalously high increase in specific heat capacity (14.5%) of a suspension of silica nanoparticles (1 wt.%) in a high-temperature alkali salt eutectic. The mechanisms suggested to explain the increased heat capacity are similar to the mechanisms suggested for thermal conductivity enhancements; namely, the existence of a semi-solid interfacial layer. The anomalous results have not been confirmed by other investigators. Nevertheless, if the existence of a substantial interfacial layer with distinct thermophysical properties can be experimentally verified, the effect can be significant in nanofluids because of the high surface-to-volume ratio of nanoparticles.

A related but distinct approach to enhancing the specific heat of heat transfer fluids has been to suspend phase-change particles in the basefluid [79]. Micron-sized encapsulated phase-change materials (mePCMs) are most commonly composed of a wax or organic inner core and a polymer-based outer shell; paraffin is the most common inner core material because of its relatively high latent heat, low vapor pressure, negligible supercooling, and chemical stability [77]. When suspended in a heat transfer fluid, PCMs serve to increase the effective heat capacity of a fluid over a relatively small temperature range as the inner core undergoes melting or phase-change. Unlike the study of nanofluids, thermophysical properties of mePCMs are well-described through a conventional understanding of mixtures. They have been successfully commercialized in specialized thermal management applications; however, in convective heat transfer applications, mePCM suspensions suffer from problems related to low thermal conductivity [77], damage of the encapsulation material [80], clogging, and increased pumping costs. At present, they have not been successfully integrated in mid or high-temperature solar thermal applications because of these drawbacks and also because they are limited to low temperatures.

Recent work on phase-change material suspensions has aimed to make nano-sized PCM particles to circumvent the practical issues associated with micro-encapsulated PCMs. Nano-encapsulated PCMs (nePCMs) have been synthesized and characterized [80]; however, since the encapsulation layer scales with the surface area of the particles, it constitutes a significant fraction of the mass which limits their effectiveness. To avoid the issues with encapsulation, Han *et al.* [81] synthesized an encapsulation free, suspension of phase-changing indium (melting temperature, 157 ^{o}C) using a dispersant to stabilize the suspensions and reduce coagulation. The use of encapsulation free phase-change nanofluids to simultaneously enhance thermal conductivity and effective heat capacity is an interesting approach but practical issues with fluid stability and lifetime remain a concern.

6.1.4 Radiative Properties

The radiative properties of nanofluids are dependent on both the basefluid and the nanoparticles. Potentially serving as basefluids, certain heat transfer fluids were found to be highly transparent for wavelengths in the solar spectrum such as molten salts [82], water, ethylene glycol, propylene glycol and Therminol® VP-1 [83]. Nanoparticles, on the other hand, can exhibit strong and tunable absorption peaks. As a first order approximation, investigators have proposed that the nanofluid absorption coefficient can be described using a simple addition of the basefluid absorption coefficient and that of the particles [84].

The radiative properties of nanoparticles are in principle well-described by Mie theory [85] when the surrounding is non-absorbing and the volume fraction is low ($\phi << 0.01$). A nanoparticle in a dielectric medium exhibits a resonant absorption peak when the frequency of the incoming light coincides with a plasmon resonant mode (*i.e.*, collective oscillation of the conduction band electrons) [86]. If the nanoparticle is indeed much smaller than the wavelength of incident light, absorption due to the particle is much stronger than scattering and is proportional to the volume of the particle [85, 87]. Hu *et al*. [88] extended the analysis by Bohren and Huffman [85] to describe nanoparticles in an absorbing medium by treating the optical constant of the host medium (*i.e.*, basefluid) as a complex number. Recently a quantum mechanical simulation has been used to validate that this description is applicable down to 10 nm in silver nanoparticles

[89] as long as the optical properties of the bulk solid are modified to account for electron scattering by the interface when describing smaller nanoparticles. In metallic nanoparticles, the dominant resonant absorption peak typically occurs in the visible spectrum but can be modified by varying the particle size, shape or shell material. Cole *et al.* proposed that a combination of as little as three metallic nanoparticles types can selectively absorb the majority of the solar spectrum [90]; in this case, the optimized composition of nanoparticles was found to contain nanospheres and nanoshells ranging from 32 nm to 58 nm.

Plasmon resonant absorption peaks for nanoparticles in suspension have been experimentally demonstrated for a range of nanoparticle materials, shapes and sizes [91]. The experimental results match well with theory as long as the particles are sufficiently dispersed such that they can be treated as isolated. Recently, however, Taylor *et al*. [84] did not observe plasmon peaks using silver nanoparticles and attributed this result in part to the presence of impurities and particle aggregates leading to increased scattering. Thus, in order for nanofluids to maintain the sharp absorption peaks and have good absorption characteristics with solar light, care must be taken to avoid agglomeration; nevertheless, more research in this area is required. Moreover, the infrared properties of high temperature pure heat transfer fluids and nanofluids, critical for understanding their thermal emissivity, have not yet been fully characterized. The application for solar absorbing nanofluids will be described further in the following section.

6.2 APPLICATIONS

So far we have focused on recent experiments and understanding the thermophysical properties of nanofluids. For heat transfer applications, it is important to consider how those properties couple together in particular applications. The heat transfer performance of nanofluids will primarily be evaluated for forced convection in solar thermal systems. We will also consider direct absorption of solar radiation by the nanofluids for concentrated solar systems using volumetric receivers.

DOI: 10.1615/AnnualRevHeatTransfer.2012004122
SOURCE: Lenert, Andrej, Youngsuk Nam, and Evelyn N. Wang. "Heat Transfer Fluids." Annual Review of Heat Transfer 15, 2012.

6.2.1 Forced Convection Heat Transfer

In convective heat transfer, the thermal performance of the nanofluid depends not only on the thermal conductivity but also on the density, viscosity, heat capacity and other dynamic mechanisms.

Investigators have shown that the heat transfer enhancements (compared to the pure basefluid) under turbulent forced flow conditions are typically between 15-45% [60]. However, Yu *et al.* [92] noticed that most of the previously reported heat transfer enhancements are based on a constant *Re* number such that the enhancement increases with increasing viscosity. When compared on the more practical basis of constant pumping power or constant velocity, only a small fraction (<30%) of studies report a forced convection heat transfer coefficient greater than that of their basefluid [92].

This result is not surprising since it was discussed in the Section 6.1 that the thermal conductivity of nanofluids does not significantly exceed the predictions of the generalized effective media theory, whereas the viscosity is typically 5-10 times the value suggested by existing models shown to apply for micro-particle suspensions. The viscosity increase typically surpasses any thermal conductivity enhancement such that the heat transfer performance of nanofluids in forced convection is commonly worse than for pure basefluids.

Enhancements in the heat transfer coefficient which cannot be predicted by traditional correlations such as Dittus-Boelter's (using the measured thermophysical properties of the nanofluids) are attributed to a variety of mechanisms. Buongiorno [93] theoretically investigated inertia, Brownian diffusion, thermophoresis, diffusiophoresis, Magnus effect, fluid drainage, and gravity as possible mechanisms which can produce a relative velocity between the particle and the fluid, and in turn, enhance heat transfer. The results show that only thermophoresis and Brownian diffusion were non-negligible slip mechanisms in nanofluids. An alternative explanation for the enhanced heat transfer was proposed: the viscosity of the nanofluid within the boundary layer may be significantly reduced because of the effect of the temperature gradient and thermophoresis, resulting in heat transfer enhancement [93]. Meanwhile, other studies suggest that the effects of thermophoresis and Brownian diffusion can also be neglected [72].

Timofeeva *et al.* [72] compared experimental heat transfer coefficient enhancements reported in literature [94-100] to a prediction using the Dittus-Boelter correlation based on the measured nanofluid properties (*i.e.*, without additional dynamic mechanisms), as shown in Figure 12. It was found that most of the data is well-predicted by the correlation alone and noted that larger particle suspensions generally perform the best.

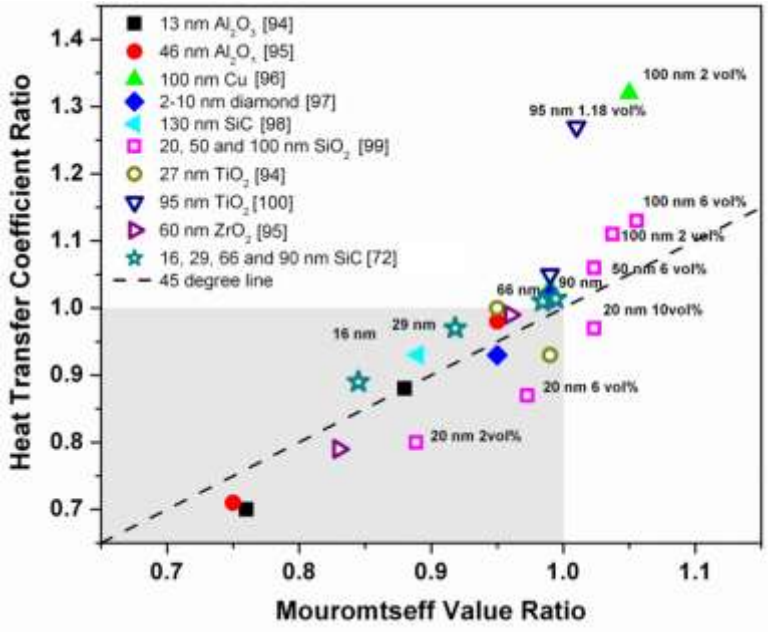

Figure 12: Experimental enhancements of turbulent heat transfer coefficient (symbols) compared to enhancement predicted based on *Mo* number using nanofluid properties (dotted line). Grey region denotes property and performance deterioration compared to pure fluid. Adapted from [72] (Copyright 2010, IOP Science).

Other investigators [77] have studied hybrid suspensions of alumina nanoparticles and mePCMs to leverage the thermal conductivity enhancement of nanofluids and storage enhancements of PCMs. However, laminar forced convection experiments in a circular tube showed that the increase in friction factor exceeds enhancements in heat transfer since the viscosity of hybrid suspensions is anomalously high.

Presently, the best performing well-dispersed nanofluids are suspensions of larger spherical particles. As compared to small and non-spherical particles, larger spherical particles provide

lower viscosity increases because of the decreased solid-liquid interfacial area [72] and reduced aggregation [101]. Practical limitations on the size of the particles are imposed by sedimentation issues. Based on these factors, studies suggested that the optimized particle size is roughly ~130 nm (diameter) [101], but the exact size is application specific.

Future work in nanofluids could lead to superior heat transfer performance, however, coupling between the different thermophysical properties of nanofluids leading to performance tradeoffs needs to be tuned and optimized.

For forced convection in solar thermal applications, the observed viscosity decrease and thermal conductivity increase with temperature makes nanofluids promising for higher temperature applications [74]. However, further studies on the performance and material stability of nanofluids at high temperatures are needed. Moreover, further research needs to be conducted on additives to stabilize and lower the viscosity of nanofluids at high temperatures. Surfactants cannot currently withstand high temperatures, while using pH to prevent agglomeration may lead to corrosion issues.

6.2.2 Volumetric Receivers

Absorbing surfaces are most commonly used to convert solar energy from its radiative form into thermal energy in existing solar thermal technologies. However, at high levels of solar concentration, a large temperature difference between the absorber and the fluid arises depending on the effectiveness of the heat transfer. This temperature difference results in substantial emissive losses owing to the quartic dependence of thermal re-radiation on the absorber temperature. Alternatively, in a volumetric receiver design, concentrated solar radiation is directly absorbed and more uniformly distributed in the surrounding fluid, decreasing the temperature difference between the absorber and the fluid.

Nanofluid volumetric receivers, where nanoparticles in a liquid medium directly absorb solar radiation, promise increased performance over surface-based receivers by minimizing temperature differences between the absorber and the fluid. Several investigators have experimentally demonstrated that nanofluids are suitable solar absorbers [102, 103]. The

radiative properties of the nanofluid can be tuned by adjusting the nanoparticle loading to achieve a balance between the distribution of heat throughout the fluid (*i.e.*, elimination of hotspots) and near-100% absorption of solar light, known as the optimum optical thickness [103]. Numerical studies showed that volumetric receivers are more efficient at higher levels of solar concentration and with increasing thickness of the absorbing nanofluid layer. As a result of the high solar-to-thermal efficiencies at high temperatures, predicted optimum receiver-side efficiencies of CSP plants utilizing nanofluid volumetric receivers exceed 35% [103]. From a practical standpoint, absorbing nanofluids are best suited for grounded solar receivers with integrated storage where a "reflective tower" [104] or hillside mounted heliostats [82] are used to beam down concentrated solar radiation into the nanofluid.

Similarly to ceramic-metallic (*i.e.*, cermet) surface absorbers, nanofluids have the potential to be spectrally selective if the basefluid is non-absorbing in the near and mid infrared (IR), while the absorbing particles are tuned to the solar spectrum. However, selective nanofluid absorbers have not yet been demonstrated. Furthermore, the stability of the nanofluid radiative properties with prolonged exposure to concentrated solar radiation and cycling in a high temperature thermal system requires more investigation.

6.3 SUMMARY & OUTLOOK

The use of submicron particles in solar thermal systems is a promising method of achieving heat transfer and storage enhancements, however, concerns related to increased pumping power, material compatibility, and additional cost are currently preventing their widespread use.

The following fundamental areas need to be further explored to improve our understanding of nanofluids: characterization and understanding of the interfacial resistance and the interfacial semi-solid layer; systematic control, characterization and understanding of particle agglomeration and its effects on thermophysical properties and heat transfer performance; and, quantitative and predictive models of nanofluid viscosity. The high-temperature heat transfer performance and material stability of nanofluids needs to be realized before they are successfully adopted in solar thermal applications.

DOI: 10.1615/AnnualRevHeatTransfer.2012004122
SOURCE: Lenert, Andrej, Youngsuk Nam, and Evelyn N. Wang. "Heat Transfer Fluids." Annual Review of Heat Transfer 15, 2012.

7. **Summary**

The development of heat transfer fluids is essential to the feasibility and efficiency of solar thermal power plants, as it determines the thermal and hydraulic performance of the collector field. In this chapter, the performance of heat transfer fluids was determined by a combination of thermophysical properties rather than by each of the individual properties. Following the work of Murakami and Mikić [4], we derived a figure of merit:

$$FOM = \frac{\rho^{2.0} c_p^{1.6} k^{1.8}}{\mu^{1.4}}$$

based on the assumption of forced turbulent convection inside a uniformly heated collector tube. The new FOM combines the effects of the thermal storage capacity of the fluid, the convective heat transfer from the walls to the fluid, and the hydraulic performance characterized by the pumping power. When evaluated based on this FOM, commonly-used heat transfer fluids generally performed as follows (in order of decreasing FOM): liquid metals, molten salts, oils, and gases. Water was found to be an exceptional heat transfer fluid considering its wide operating temperature range and additional increase in volumetric heat capacity during vaporization. The use of water as a heat transfer fluid for direct steam generation (DSG) is a promising method to increase the efficiency and reduce cost of solar plants because of the high temperature output and the elimination of a heat exchange process. However, system components including the power block, the water-steam separator and the control scheme need to be carefully designed. New developments in the field of mixtures, such as multi-component salts and ionic liquids, and composite fluids, such as nanofluids, were reviewed and discussed. Liquidus temperatures well below 100^{o}C have been demonstrated using inorganic multi-component salt mixtures (nitrite/nitrate mixtures of Li, Na, K). Ionic liquids were found to have wider temperature ranges than existing synthetic oils used in CSP, but challenges with high viscosity and high cost need to be addressed. Finally, heat transfer enhancements in nanofluids were explored. On the basis of constant pumping power or constant velocity, only a small fraction (<30%) of nanofluids studies report an enhancement in the forced convection heat transfer coefficient compared to the basefluid. Within practical limits, the best performing well-dispersed nanofluids are suspensions of larger spherical particles (~100 nm) since they have lower viscosities as compared to suspensions of small and non-spherical particles.

Acknowledgements

The authors of this chapter thank the King Fahd University of Petroleum and Minerals in Dhahran, Saudi Arabia, for partially funding the research reported in this paper through the Center for Clean Water and Clean Energy at MIT and KFUPM under PROJECT NUMBER 6918351. The authors would also like to acknowledge Alban C. Cobi for compiling the data presented in *Section 3: Conventional Heat Transfer Fluids*. Andrej Lenert acknowledges the support of the National Science Foundation Graduate Fellowship. Youngsuk Nam was supported as part of the S3TEC Center, an Energy Frontier Research Center funded by the U.S. Department of Energy, Office of Science, Office of Basic Energy Sciences under Award Number DE-SC0001299.

References

1. M. Becker, Comparison of Heat Transfer Fluids for Use in Solar Thermal Power Stations, **Electric Power Systems Research**, Vol. 3(3-4), pp. 139-150, 1980.
2. I.E. Mouromtseff, Water and Forced Air Cooling of Vacuum Tubes, **Proceedings of the IRE**, Vol. 30(4), pp. 190-205, 1942.
3. C.F. Bonilla, **Nuclear Engineering**, McGraw-Hill Book Company, Inc., New York, 1957.
4. Y. Murakami and B.B. Mikic, Parametric Optimization of Multichanneled Heat Sinks for VLSI Chip Cooling, **Components and Packaging Technologies, IEEE Transactions on**, Vol. 24(1), pp. 2-9, 2001.
5. W.H. McAdams, **Heat Transmission**, McGraw-Hill, New York, 1954.
6. F.W. Dittus and L.M.K. Boelter, Heat Transfer in Automobile Radiators of the Tubular Type, **University of California Publications in Engineering**, Vol. 2, pp. 443-461, 1930.
7. D. Kearney, Solar Electric Generating Stations (SEGS), **Power Engineering Review, IEEE**, Vol. 9(8), pp. 4-8, 1989.
8. L. Moens and D. Blake, "Mechanism of Hydrogen Formation in Solar Parabolic Trough Receivers," NREL/TP-510-42468, Golden, 2008.
9. D. Kearney et al., Engineering Aspects of a Molten Salt Heat Transfer Fluid in a Trough Solar Field, **Energy**, Vol. 29(5-6), pp. 861-870, 2004.
10. Solutia Inc., "Therminol® VP-1."
11. L.L.C. Coastal Chemical Co., "Hitec® Heat Transfer Salt."
12. M.S. Sohal et al., "Engineering Database of Liquid Salt Thermophysical and Thermochemical Properties," INL/Ext-10-18297, 2010, from: www.inl.gov.
13. Global Digital Central, "Thermal-Fluids Central," from: www.thermalfluidscentral.org.
14. NIST, "Thermophysical Properties of Fluid Systems," from: www.nist.gov/srd/nsrds.cfm
15. N.B. Vargaftik et al., **Handbook of Physical Properties of Liquids and Gases: Pure Substances and Mixtures**, Begell House, New York, 1996.

16. J.G. Cordaro, N.C. Rubin, and R.W. Bradshaw, Multicomponent Molten Salt Mixtures Based on Nitrate/Nitrite Anions, **Journal of Solar Energy Engineering**, Vol. 133, pp. 011014:1-4, 2011.
17. E. Zarza et al., Direct Steam Generation in Parabolic Troughs: Final Results and Conclusions of the DISS Project, **Energy**, Vol. 29(5-6), pp. 635-644, 2004.
18. S.H. Pawar and L.A. Ekal, **Advances in Renewable Energy Technologies**, Narosa Pub. House, New Delhi, 2003.
19. D. Mills, Advances in Solar Thermal Electricity Technology, **Solar Energy**, Vol. 76(1-3), pp. 19, 2001.
20. P. Hank et al., Advances in Parabolic Trough Solar Power Technology, **Journal of Solar Energy Engineering**, Vol. 124(2), pp. 109-125, 2002.
21. M. Eck and W.D. Steinmann, Direct Steam Generation in Parabolic Troughs: First Results of the DISS Project, **Journal of Solar Energy Engineering**, Vol. 124(2), pp. 134-139, 2002.
22. E. Zarza et al., The DISS Project: Direct Steam Generation in Parabolic Trough Systems. Operation and Maintenance Experience and Update on Project Status, **Journal of Solar Energy Engineering**, Vol. 124(2), pp. 126-133, 2002.
23. E. Zarza et al., INDITEP: The First Pre-Commercial DSG Solar Power Plant, **Solar Energy**, Vol. 80(10), pp. 1270, 2006.
24. M. Eck et al., Applied Research Concerning the Direct Steam Generation in Parabolic Troughs, **Solar Energy**, Vol. 74(4), pp. 341-351, 2003.
25. L. Valenzuela et al., Control Concepts for Direct Steam Generation in Parabolic Troughs, **Solar Energy**, Vol. 78(2), pp. 301, 2005.
26. M. Eck and M. Eberl, "Controller Design for Injection Mode Driven Direct Solar Steam Generating Parabolic Trough Collectors," ISES Solar World Congress, Vol. I, pp. 247-257, 1999.
27. D. Butterworth and D.J. Pulling, "A visual study of mechanisms in horizontal, annular, air–water flow**,"** AERE-M2556, 1972.
28. S.D. Odeh, M. Behnia, and G.L. Morrison, Hydrodynamic Analysis of Direct Steam Generation Solar Collectors, **Journal of Solar Energy Engineering**, Vol. 122(1), pp. 14-22, 2000.
29. Y. Taitel and A.E. Dukler, A Model for Predicting Flow Regime Transitions in Horizontal and near Horizontal Gas-Liquid Flow, **AIChE Journal**, Vol. 22(1), pp. 47, 1976.
30. M. Eck and W.D. Steinmann, Modeling and Design of Direct Solar Steam Generating Collector Fields, **Journal of Solar Energy Engineering**, Vol. 127(3), pp. 371-380, 2005.
31. M.M. Shah, "Chart Correlation for Saturated Boiling Heat Transfer: Equations and Further Study," Semi-annual meeting of the American Society of Heating, Refrigerating, and Air Conditioning Engineers, Houston, 1982.
32. R.C. Martinelli and D.B. Nelson, Prediction of Pressure Drop During Forced Circulation Boiling of Water, **Trans. ASME**, Vol. 70, pp. 695-702, 1948.
33. K.E. Gungor and R.H.S. Winterton, A General Correlation for Flow Boiling in Tubes and Annuli, **International Journal of Heat and Mass Transfer**, Vol. 29(3), pp. 351, 1986.
34. J.C. Chen, Correlation for Boiling Heat Transfer to Saturated Fluids in Convective Flow, **Industrial & Engineering Chemistry Process Design and Development**, Vol. 5(3), pp. 322, 1966.

35. H.K. Forster and N. Zuber, Dynamics of Vapor Bubbles and Boiling Heat Transfer, **AIChE Journal**, Vol. 1(4), pp. 531, 1955.
36. D.L. Bennett, M.W. Davis, and B.L. Hertzler, The Suppression of Saturated Nucleate Boiling by Forced Convection Flow, **AIChE Symposium Series**, Vol. 76, pp. 91–103, 1980.
37. S.G. Kandlikar, A General Correlation for Saturated Two-Phase Flow Boiling Heat Transfer inside Horizontal and Vertical Tubes, **Journal of Heat Transfer**, Vol. 112, pp. 219-228, 1990.
38. S.D. Odeh, G.L. Morrison, and M. Behnia, Modeling of Parabolic Trough Direct Steam Generation Solar Collectors, **Solar Energy**, Vol. 62, pp. 395-406, 1998.
39. M.E. Rojas, M.C. de Andrés, and L. González, Designing Capillary Systems to Enhance Heat Transfer in LS3 Parabolic Trough Collectors for Direct Steam Generation (DSG), **Solar Energy**, Vol. 82(1), pp. 53, 2008.
40. L. Friedel, "Improved Friction Pressure Drop Correlations for Horizontal and Vertical Two Phase Pipe Flow," European Two Phase Flow Group Meeting, Isra, 1979.
41. J.R. Thome, **Engineering Data Book III**, Wolverine Tube Inc., Lausanne, 2004.
42. R.W. Lockhart and R.C. Martinelli, Proposed Correlation of Data for Isothermal Two-Phase Two-Component Flow in Pipes, **Chem. Eng. Prog.**, Vol. 45, pp. 39-45, 1949.
43. J.M. Chawla, Wärmeübergang Und Druckabfall in Waagerechten Rohren Bei Der Strömung Von Verdampfenden Kältemitteln, **VDI-Forsch. H., VDI-Verlag Düsseldorf, FRG**, Vol., pp. 523, 1967.
44. J. Rheinlander and M. Eck, **Direct Solar Steam (DISS) Numerical Modeling of Pressure Losses,** 2002.
45. P.R.H. Blasius, Das Aehnlichkeitsgesetz bei Reibungsvorgangen in Flüssigkeiten, **Forschungsheft,** Vol. 131**,** pp. 1-41, 1913.
46. E. Dagan, M. Muller, and F. Lippke, "Direct Steam Generation in the Parabolic Trough Collector," Report of Plataforma Solar De Almeria, 1992.
47. F. Jan Fabian et al., Economic Potential of Solar Thermal Power Plants with Direct Steam Generation Compared with Htf Plants, **Journal of Solar Energy Engineering**, Vol. 132(4), pp. 041001.
48. L. Moens et al., Advanced Thermal Storage Fluids for Solar Parabolic Trough Systems, **Journal of Solar Energy Engineering**, Vol. 125(1), pp. 112-116, 2003.
49. M.E. Van Valkenburg et al., "Ionic Liquid Heat Transfer Fluids," Fifteenth Symposium on Thermophysical Properties, Boulder, 2003.
50. G.J. Janz, **Molten Salts Handbook**, Academic Press, New York, 1967.
51. R.W. Bradshaw, J.G. Cordaro, and N.P. Siegel, "Molten Nitrate Salt Development for Thermal Energy Storage in Parabolic Trough Solar Power Systems," ASME 3rd International Conference on Energy Sustainability, Vol. 2, pp. 615-624, 2009.
52. K.R. Seddon, Ionic Liquids for Clean Technology, **Journal of Chemical Technology & Biotechnology**, Vol. 68(4), pp. 351, 1997.
53. C.P. Fredlake et al., Thermophysical Properties of Imidazolium-Based Ionic Liquids, **Journal of Chemical & Engineering Data**, Vol. 49(4), pp. 954, 2004.
54. M.E.V. Van Valkenburg et al., Thermochemistry of Ionic Liquid Heat-Transfer Fluids, **Thermochimica Acta**, Vol. 425(1-2), pp. 181-188, 2005.

55. H. Chen et al., Rheological and Heat Transfer Behaviour of the Ionic Liquid, [C4mim][Ntf2], **International Journal of Heat and Fluid Flow**, Vol. 29(1), pp. 149, 2008.
56. J.C. Maxwell, **A Treatise on Electricity and Magnetism**, Oxford, Clarendon, 1881.
57. P. Keblinski, J.A. Eastman, and D.G. Cahill, Nanofluids for Thermal Transport, **Materials Today**, Vol. 8(6), pp. 36, 2005.
58. S.K. Das, S.U.S. Choi, and H.E. Patel, Heat Transfer in Nanofluids - a Review, **Heat Transfer Engineering**, Vol. 27(10), pp. 3 - 19, 2006.
59. X.-Q. Wang and A.S. Mujumdar, Heat Transfer Characteristics of Nanofluids: A Review, **International Journal of Thermal Sciences**, Vol. 46(1), pp. 1, 2007.
60. W. Yu et al., Review and Comparison of Nanofluid Thermal Conductivity and Heat Transfer Enhancements, **Heat Transfer Engineering**, Vol. 29(5), pp. 432 - 460, 2008.
61. C. Kleinstreuer and Y. Feng, Experimental and Theoretical Studies of Nanofluid Thermal Conductivity Enhancement: A Review, **Nanoscale Research Letters**, Vol. 6(1), pp. 229, 2011.
62. S.H. Oh et al., Ordered Liquid Aluminum at the Interface with Sapphire, **Science**, Vol. 310(5748), pp. 661-663, 2005.
63. W.D. Kaplan and Y. Kauffmann, Structural Order in Liquids Induced by Interfaces with Crystals, **Annual Review of Materials Research**, Vol. 36(1), pp. 1-48, 2006.
64. C. Gerardi et al., Nuclear Magnetic Resonance-Based Study of Ordered Layering on the Surface of Alumina Nanoparticles in Water, **Applied Physics Letters**, Vol. 95, pp. 253104, 2009.
65. E.V. Timofeeva, J.L. Routbort, and D. Singh, Particle Shape Effects on Thermophysical Properties of Alumina Nanofluids, **Journal of Applied Physics**, Vol. 106(1), pp. 014304, 2009.
66. C.T. Wamkam et al., Effects of Ph on Heat Transfer Nanofluids Containing Zro_2 and Tio_2 Nanoparticles, **Journal of Applied Physics**, Vol. 109(2), pp. 024305, 2011.
67. P. Keblinski et al., Mechanisms of Heat Flow in Suspensions of Nano-Sized Particles (Nanofluids), **International Journal of Heat and Mass Transfer**, Vol. 45(4), pp. 855, 2002.
68. J. Buongiorno et al., A Benchmark Study on the Thermal Conductivity of Nanofluids, **Journal of Applied Physics**, Vol. 106(9), 2009.
69. C.W. Nan et al., Effective Thermal Conductivity of Particulate Composites with Interfacial Thermal Resistance, **Journal of Applied Physics**, Vol. 81(10), pp. 6692-6699, 1997.
70. D.C. Venerus et al., Viscosity Measurements on Colloidal Dispersions (Nanofluids) for Heat Transfer Applications, **Applied Rheology**, Vol. 20(4), 2010.
71. A. Einstein, Eine Neue Bestimmung Der Moleküldimensionen, **Annalen der Physik**, Vol. 324(2), pp. 289, 1906.
72. E.V. Timofeeva et al., Particle Size and Interfacial Effects on Thermo-Physical and Heat Transfer Characteristics of Water-Based Alpha-SiC Nanofluids, **Nanotechnology**, Vol. 21(21), pp. 215703, 2010.
73. K.B. Anoop et al., Rheological and Flow Characteristics of Nanofluids: Influence of Electroviscous Effects and Particle Agglomeration, **Journal of Applied Physics**, Vol. 106(3), pp. 034909, 2009.

74. E. Timofeeva et al., Nanofluids for Heat Transfer: An Engineering Approach, **Nanoscale Research Letters**, Vol. 6(1), pp. 182, 2011.
75. G. Cao, **Nanostructures & Nanomaterials: Synthesis, Properties & Applications**, Imperial College Press, London, 2004.
76. T.L. Bergman, Effect of Reduced Specific Heats of Nanofluids on Single Phase, Laminar Internal Forced Convection, **International Journal of Heat and Mass Transfer**, Vol. 52(5-6), pp. 1240, 2009.
77. C.J. Ho et al., On Laminar Convective Cooling Performance of Hybrid Water-Based Suspensions of Al_2o_3 Nanoparticles and Mepcm Particles in a Circular Tube, **International Journal of Heat and Mass Transfer**, Vol. 54(11-12), pp. 2397, 2011.
78. D. Shin and D. Banerjee, Enhancement of Specific Heat Capacity of High-Temperature Silica-Nanofluids Synthesized in Alkali Chloride Salt Eutectics for Solar Thermal-Energy Storage Applications, **International Journal of Heat and Mass Transfer**, Vol. 54(5-6), pp. 1064, 2010.
79. K.E. Kasza and M.M. Chen, Improvement of the Performance of Solar Energy or Waste Heat Utilization Systems by Using Phase-Change Slurry as an Enhanced Heat-Transfer Storage Fluid, **Journal of Solar Energy Engineering**, Vol. 107(3), pp. 229-236, 1985.
80. G. Fang et al., Preparation and Characterization of Nano-Encapsulated N-Tetradecane as Phase Change Material for Thermal Energy Storage, **Chemical Engineering Journal**, Vol. 153(1-3), pp. 217, 2009.
81. Z.H. Han, F.Y. Cao, and B. Yang, Synthesis and Thermal Characterization of Phase-Changeable Indium/Polyalphaolefin Nanofluids, **Applied Physics Letters**, Vol. 92(24), pp. 243104, 2008.
82. A.H. Slocum et al., Concentrated Solar Power on Demand, **Solar Energy**, Vol. 85(7), pp. 1519-1529, 2011.
83. T.P. Otanicar, P.E. Phelan, and J.S. Golden, Optical Properties of Liquids for Direct Absorption Solar Thermal Energy Systems, **Solar Energy**, Vol., 2009.
84. R. Taylor et al., Nanofluid Optical Property Characterization: Towards Efficient Direct Absorption Solar Collectors, **Nanoscale Research Letters**, Vol. 6(1), pp. 225, 2011.
85. C.F. Bohren and D.R. Huffman, **Absorption and Scattering of Light by Small Particles**, Wiley-VCH, New York, 1998.
86. U. Kreibig and M. Vollmer, **Optical Properties of Metal Clusters**, Springer, Berlin Heidelberg, 1995.
87. M.F. Modest, **Radiative Heat Transfer**, Second ed, Academic Press, Burlington, 2003.
88. L. Hu, X. Chen, and G. Chen, Surface-Plasmon Enhanced near-Bandgap Light Absorption in Silicon Photovoltaics, **Journal of Computational and Theoretical Nanoscience**, Vol. 5, pp. 2096, 2008.
89. Y. He and T. Zeng, First-Principles Study and Model of Dielectric Functions of Silver Nanoparticles, **The Journal of Physical Chemistry C**, Vol. 114(42), pp. 18023, 2010.
90. J.R. Cole and N.J. Halas, Optimized Plasmonic Nanoparticle Distributions for Solar Spectrum Harvesting, **Applied Physics Letters**, Vol. 89(15), pp. 153120, 2006.
91. K.L. Kelly et al., The Optical Properties of Metal Nanoparticles: The Influence of Size, Shape, and Dielectric Environment, **The Journal of Physical Chemistry B**, Vol. 107(3), pp. 668, 2002.

92. W. Yu et al., Thermophysical Property-Related Comparison Criteria for Nanofluid Heat Transfer Enhancement in Turbulent Flow, **Applied Physics Letters**, Vol. 96(21), pp. 213109, 2010.
93. J. Buongiorno, Convective Transport in Nanofluids, **Journal of Heat Transfer**, Vol. 128(3), pp. 240-250, 2006.
94. B.C. Pak and Y.I. Cho, Hydrodynamic and Heat Transfer Study of Dispersed Fluids with Submicron Metallic Oxide Particles, **Experimental Heat Transfer**, Vol. 11(2), pp. 151 - 170, 1998.
95. W. Williams, J. Buongiorno, and L.-W. Hu, Experimental Investigation of Turbulent Convective Heat Transfer and Pressure Loss of Alumina/Water and Zirconia/Water Nanoparticle Colloids (Nanofluids) in Horizontal Tubes, **Journal of Heat Transfer**, Vol. 130(4), pp. 042412, 2008.
96. Y. Xuan and Q. Li, Investigation on Convective Heat Transfer and Flow Features of Nanofluids, **Journal of Heat Transfer**, Vol. 125(1), pp. 151-155, 2003.
97. S. Torii and W.-J. Yang, Heat Transfer Augmentation of Aqueous Suspensions of Nanodiamonds in Turbulent Pipe Flow, **Journal of Heat Transfer**, Vol. 131(4), pp. 043203, 2009.
98. W. Yu et al., Heat Transfer to a Silicon Carbide/Water Nanofluid, **International Journal of Heat and Mass Transfer**, Vol. 52(15-16), pp. 3606, 2009.
99. D.P. Kulkarni et al., Convective Heat Transfer and Fluid Dynamic Characteristics of Sio_2 Ethylene Glycol/Water Nanofluid, **Heat Transfer Engineering**, Vol. 29(12), pp. 1027 - 1035, 2008.
100. Y. He et al., Heat Transfer and Flow Behaviour of Aqueous Suspensions of Tio2 Nanoparticles (Nanofluids) Flowing Upward through a Vertical Pipe, **International Journal of Heat and Mass Transfer**, Vol. 50(11-12), pp. 2272, 2007.
101. P.E. Gharagozloo and K.E. Goodson, Temperature-Dependent Aggregation and Diffusion in Nanofluids, **International Journal of Heat and Mass Transfer**, Vol. 54(4), pp. 797, 2011.
102. T.P. Otanicar et al., Nanofluid-Based Direct Absorption Solar Collector, **Journal of Renewable and Sustainable Energy**, Vol. 2(3), pp. 033102, 2010.
103. A. Lenert and E.N. Wang, Optimization of Nanofluid Volumetric Receivers for Solar Thermal Energy Conversion, **Solar Energy**, Vol. 86(1), pp. 253-265, 2012.
104. M. Epstein, A. Segal, and A. Yogev, A Molten Salt System with a Ground Base-Integrated Solar Receiver Storage Tank, **J. Phys. IV France**, Vol. 09(PR3), pp. 95-104, 1999.